Journal of Petroleum & Environmental Biotechnology

GUO, J Pet Environ Biotechnol 2011, 2:3
DOI: 10.4172/2157-7463.1000112

Research Article Open Access

Membranes Coupled with Nanotechnology for Daily Drinking Water: an Overview

Kelvii Wei GUO*

Department of Mechanical and Biomedical Engineering, City University of Hong Kong, 83 Tat Chee Avenue, Kowloon Tong, Kowloon, China

Abstract

It is well known that current global development is not sustainable over the long term. Every major ecosystem is under threat at different timescales, impacting water, food, energy, biodiversity, and mineral resources—all exacerbated by the population growth and climate change.Potable water is a threatened but critical resource, the scarcity of which isdevastating for the developing world. Water-related nanotechnology researchhas the potential to make safe drinking water inexpensive and accessible todeveloping countries. Therefore, the relevant nanotechnologies on membranes for filtrating drinking water are reviewed. At the same time, it is pointed out that for the foressable future membranes must exhibit a number ofcharacteristics such as high water flux, high salt rejection, mechanical stability,resistance to fouling, and low cost. With new breakthroughs in membrane technology, constituent specificmembranes should be realized andthe promising reverse osmosis membranes coupled with new nanotech will be applicable tonanofiltration membranes in the future.

Keywords: Membrane; Nanotechnology; Drinking water; Nanostructure; Nanoparticle; CNTs.

Introduction

It is well known that current global development is not sustainable over the long term. Every major ecosystem is under threat at different timescales, impacting water, food, energy, biodiversity, and mineral resources—all exacerbated by the population growth and climate change. It has been estimated that about 1.1 billion people are now at risk from a lack of clean water and about 35 percent of people in the developing world die from water-related problems [1,2]. Also, aquifers throughout around the world are suffering from declining water levels, saltwater intrusion, contamination from surface waters, and inadequately replenished fresh groundwater. Major rivers and watersheds are also being overdrawn, while return flows are contributing to downstream nutrient loading and salinity problems. Lakes and wetlands are also experiencing increased salting in many areas. Furthermore, as increases in acreage and irrigation are needed for the production of biofuels, further dramatic increases in demand will strain existing water supplies and new water sources will be needed. If lack of water limits growth in new energy supplies, every aspect of the global economy will be affected, increasing costs to the consumer. Clearly, the costs to upgrade infrastructure and create new supplies likely cannot be met without revolutionary improvements in the science and technology of water purification. Because water is a ubiquitous facilitator of civilization, *de facto* essential for almost everything, ranging from maintaining human health, to ensuring plant growth, and enabling the transport of merchandise, ensuring adequate supplies of potable water for human use must continue to be a research priority, the environmental impacts of increasing human water consumption will also demand attention. Moreover, better research on the availability, detection of contaminants, and strategies for remediation can increase utilization of currently available sources as well as facilitate development of new water sources such as brackish aquifers. At the same time, depending on the new generation and cooling technology deployed, fresh water consumption is expected to increase more. Concurrent efforts to reduce dependence on imported oil through new fuels such as biomass, syngas, and hydrogen are expected to expand the overall water footprint of the energy sector even further. New sources of water, and new purification technologies to enhance water reuse, will be needed to keep pace with energy demands. Also, food production is even more closely linked to the availability of water than energy production. New technologies that can dramatically enhance agricultural water conservation and increase the recovery and reuse of irrigation runoff and livestock waste water could have the largest impact on future water availability [3-5].

Recently, water supply has also emerged as a high-value target for terrorism. Disabling and/or contamination of urban water distribution systems can impact thousands, and in some cases, millions of customers, and the inherently open nature of wastewater collection systems renders them vulnerable to the weaponization of a myriad of commercial and industrial chemicals [6,7].

To date, it should be noted that lack of access to potable water is a leading cause of death worldwide .Dehydration, diarrheal diseases, contaminated source waters, water borne pathogens, water needed for food production (starvation), and water for sanitation are just some of the factors that impact health. The water-health nexus is crucial for the survival of humanity. Creating better disinfection and purification technologies could significantly reduce these problems that much of the world currently faces and equally importantly, some regions of the developed world may soon face [8,9].

Meanwhile, people all over the world face profound threats to the availability of sufficient safe and clean water, affecting their health and economic well-being. The problems with economically providing clean

***Corresponding author:** Kelvii Wei GUO, Department of Mechanical and Biomedical Engineering, City University of Hong Kong, 83 Tat Chee Avenue, Kowloon Tong, Kowloon, China, E-mail: kelviiguo@yahoo.com

Received August 23, 2011; **Accepted** November 17, 2011; **Published** November 19, 2011

Citation: GUO KW (2011) Membranes Coupled with Nanotechnology for Daily Drinking Water: an Overview. J Pet Environ Biotechnol 2:112. doi:10.4172/2157-7463.1000112

water are growing so quickly that incremental improvements in current methods of water purification could leave much of the world with inadequate supplies of clean water in mere decades. The challenges to overcome in science, technology, and society require a long term vision of what needs to be solved [9-13].

Therefore, ensuring the availability of clean, abundant fresh water for human use is among the most pressing issues facing the world. It is stated over the next two decades, the average supply of water per person will drop by a third, possibly condemning millions of people to an avoidable premature death, and environmental stress resulting from climate change and population growth and migration is expected to increase over next two decades.

There is urgent that satisfying humankind's demand for water in a sustainable manner requires visionary new approaches to management and conservation of water resources augmented by new technologies capable of dramatically reducing the cost of supplying clean fresh water-technologies that can best be derived from tightly coupled basic and applied research.

Science and technology are turbulent dynamic fields where coherent structures appear and break down. Nanotechnology promises to dominate the landscape for many of these fields over the next several decades. Research and development at this scale can answer major challenges for society, from improved comprehension of nature and increased productivity in manufacturing, to molecular medicine and extending the limits for sustainable development [14-16].

Actually, for nanotechnology, a key objective is to develop materials, devices, and systems with fundamentally different properties by exploiting the unique properties of molecular and supramolecular systems at the nanoscale. In recent years, research in this field has grown exponentially as scientists and engineers continue to develop nanomaterials with unique and enhanced properties. Nearly every field of science has been affected by the tools and ideas of nanotechnology, and breakthroughs have been made in computing, medicine, sensing, energy production, and environmental protection. Recent advances strongly suggest that many of the current problems involving water quality can be addressed and potentially resolved using nanosorbents, nanocatalysts, bioactive nanoparticles, nanostructured catalytic membranes, and nanoparticle enhanced filtration, among other products and processes resulting from the development of nanotechnology [17-20].

Moreover, nanotechnology solutions are essential because the abiotic and biotic impurities most difficult to separate in water are in the nanoscale range. By its control at the foundation of matter, nanoscale science and engineering may bring breakthrough technologies possible for improving water quality. Also, on the other end, nanotechnology may offer efficient manufacturing with less resources and waste to reduce pollution at its site of origin [21-24].

It is by now presumably well known that nanotechnology has the potential to contribute novel solutions to an enormous range of problems currently facing the world. Ensuring the availability of potable water ranks as one of the more important and urgent of those problems, and nanotechnology is clearly a candidate for helping to solve it. Furthermore, nanotechnology is specifically appropriate because the problems of water purification, from the viewpoint of what needs to be removed from contaminated water, crucially mostly involve the nanoscale.

In addition, water filtration and desalinization have been relatively less-explored topics in nanotechnology, but there has been a new trend in this direction in the last few years. This is an area of importance for life, it is of significant interest to the productive engine and the public at large, and there are many stakeholders. It should be pointed out that research and development have been lagging behind advances in areas such as electronics, materials science, and pharmaceuticals, which have relatively shorter term returns. Infrastructure for water resources requires a relatively larger investment for a longer period of time and the diverse potential sponsoring sources need to be better coordinated.

Considering the problems of current drinking water, research on membranes coupled with nanotechnologyis reviewed as follows.

Membranes with functional nanoparticles

Polymers and ceramics, the two main classes of membrane materials, have distinct advantages as platforms for the design of multifunctional membranes. Due to their high chemical and thermal stability, ceramic membranes can support additional functions and processes in highly oxidizing environments and under conditions of extreme pH and temperatures. Polymers, on the other hand, offer great design flexibility and are generally less expensive. Polymeric multifunctional membranes can be prepared by modifying materials traditionally used in membrane manufacture. Surface functionalization of existing membranes and the use of block copolymers and hybrid polymers as membrane materials are examples of such methods. Another approach is that of developing new hybrid membrane materials by incorporating (metal oxide, metal, carbon, or polymeric) functional nanoparticles into the polymeric matrix [25-30].

At the same time, nanotechnology has enabled the development of a new class of atomic scale materials capable of fighting waterborne disease-causing microbes. The explosive growth in nanotechnology research has opened the doors to new strategies using nanometallic particles for oligodynamic disinfection [31-33]. The excellent microbicidal properties of the oligodynamic nanoparticles qualify their use as viable alternatives for water disinfection. Oligodynamic metallic nanoparticles such as silver, copper, zinc, titanium, nickel and cobalt are among the most promising nanomaterials with bactericidal and viricidal properties owing to their charge capacity, high surface-to-volume ratios, crystallographic structure, and adaptability to various substrates for increased contact efficiency. This new class of nanometallic particles produces antimicrobial action referred to as oligodynamic disinfection for their ability to inactivate microorganisms at low concentrations. When oligodynamic metals with microbicidal, bactericidal, and viricidal properties are reduced the size of the metals to the nanoscale, they show tremendous advantages in disinfection capacity due to the greater surface area, contact efficiency, and often better elution properties. These qualities enable these materials to be considered asviable alternative disinfectants, such as silver (Ag), copper (Cu), zinc (Zn), titanium (Ti), and cobalt (Co).New combinatorial oligodynamic materials consisting of these nanometallic particles have been deployed among a number of substrates for their use in water disinfection [34-36]. Such materials as Ag deposited on titanium oxide, and Ag-coated iron oxide had displayed faster kinetics and greater efficiency in eliminating bacteria.

Nowadays, silver is the most widely studied oligodynamic material due to its wide range in microbicidal effectiveness, low toxicity, and ease of incorporation on various substrates in a host of dynamic disinfection applications. Furthermore, the systems supported with

nanometallic silver particles are effective in reducing the presence of target microorganisms in a wide variety of water disinfection applications, except the main known negative health effect from silver is argyria, which is an irreversible darkening of the skin and mucous membrane resulting from overexposure to ionic silver (Ag(I), Ag+) [37].

Typically, the silver nanoparticles are derived from silver salts (silver nitrate ($AgNO_3$), silver chloride (AgCl), silver bromide (AgBr), and silver iodide (AgI)), and a variety of substrates that silver deployed on such as activated carbon, activated carbon fibers (ACF), polyurethane, zeolites, and ceramics in POE and POU applications displays the effective inactivation of pathogens in water [38-41]. Wang et al. [42] prepared viscose-based activated carbon fiber supporting silver (ACF(Ag)) by pretreatment, carbonization, activation, vacuum impregnation and decomposition processes, which ACFs were successively subjected to a vacuum impregnation treatment in unsaturated silver nitrate(analytical grade) aqueous ($AgNO_3$) solutions ($NH_4H_2PO_4$ 3.3 gl^{-1}, $(NH_4)_2SO_4$ 6.7 gl^{-1}) with varying concentrations for different times, and were varying concentrations for different times, and were finally heated to different temperatures for decomposition, thus producing ACF(Ag). Thereafter, the ACF (Ag) samples were ashed at 800°C for6 hours in atmosphere, the resulting ashes were then dissolved in 50 ml of 10% (vol.) HNO_3 solutions (90°C) to determine the silver content. It reveals that the silver particle size is influenced by the concentration of $AgNO_3$ solution, immersion time and decomposition temperature, of which $AgNO_3$ content is the most remarkable factor (as shown in Figure 1). Moreover, the ACF (Ag) containing as low as 0.065 wt% of silver exhibits the strong antibacterial property against *Escherichia coli* and *Staphylococcus aureus*.

Though many forms of silver have found use in disinfection applications, which include swimming pools and hospital hot water systems, silver nanoparticles find the most extant usage in POU applications including activated-carbon-based and ceramic water purification filters. POU filters composed of granular activated carbon impregnated with silver have received ample attention in the past decade owing to their high surface area and pore size distribution that allow silver to be easily entrapped in the pores and later desorbed [42,43]. Carbon-based substrates lower the impact of the silver nanoparticles. With a loading of 0.05 wt percent Ag impregnation in an ACF with extremely high surface area (1200 m^2/g), the fastest time achieved for complete bacterial elimination is 30 minutes. The silver impregnated carbon-based filters displays only bacteriostatic performance since they are not able to completely eliminate microbial regrowth in POU devices. Such performance related issues can be addressed by deploying silver nanoparticles on inorganic-based substrates and by using combinations of oligodynamic nanoparticles [43].

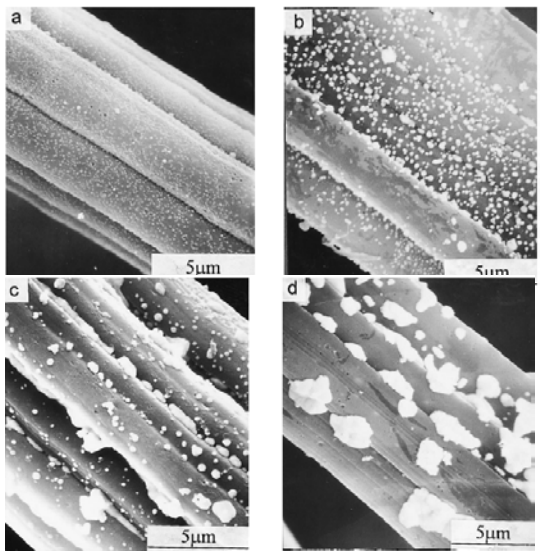

Figure 1: SEM photographs of the ACF(Ag) samples immersed in $AgNO_3$ solutions with different concentrations (a) 0.01, (b)0.1, (c) 0.4 and (d) 0.7 mol l^{-1}[42].

Nitrogen-doped titanium-oxide

Titanium oxide (TiO_2) is modified by nanoparticles of transition metal oxides and made into nanoparticles, nanoporous fibers, and nanoporous foams. The nanostructured photocatalysts show very fast photocatalytic degradation rates in organics, bacteria, spores, and virus, and thus have great potential in water disinfection and removal of organic contaminants in water. The basis for photocatalytic control is the production of highly reactive oxidants, such as OH radicals, for oxidization of organic pollutants, disinfection of microorganisms, and degradation of hazardous disinfection by-products (DBPs) and disinfection by-product precursors (DBPPs) [44-46].

With the newly developed TiON-based photocatalysts, photocatalytic degradation and disinfection can be implemented with visible light. The replacement of UV by visible light offers potential for low-cost environmental measures, especially for water treatment, where UV access is rather limited. The removal of organic contaminations has been demonstrated by the photodegradation of HA by TiON/PdO under visible-light illumination. The addition of PdO allows the electron transfer process on the photocatalyst to be "regulated" by storing and releasing electrons to minimize electron ehole recombination [47] or to produce a long-lasting photocatalytic 'memory' effect after light is turned off. While the hydroxyl radicalsgenerated by the visible light photocatalysis are believed to be the working species in bacterial inactivation [48,49]. *Escherichia coli* is a model gram negative bacterium, which is widely used as a bacterial indicator. TiON/PdO shows the high disinfection efficiency against *E. coli*. After 30min visible-light illumination, the survival ratio of *Escherichiacoli* drops to approximately 10^{-8}. Wu et al. [50] characterized the cellular responses of *Escherichia coli* to visible light photocatalysis by chemical,optical, electron-beam, and surface-force techniques, to elucidate the mechanisms of photocatalytic inactivation of *E. coli* on PdO/TiON fiber. PdO/TiON-deposited fiber photocatalyst was prepared by a mixture of titanium tetraisopropoxide and tetramethyl ammonium hydroxide (mol ratio 4:1) in absolute ethanol. Then a proper amount of Pd $(acac)_2$ dissolved in CH_2Cl_2 was added. Activated carbon-coated glass fiber (ACGF) was soaked in the precursor mixture for 24 hat room temperature. After wash and dry, fine crystallites of PdO/TiON nanoparticles deposited on fibers were obtained by calcination (400°C, 3 h), followed by removal of carbon at 500°C for 1 h in air. For viability assays, a typical procedure of photocatalytic treatment was as follows. Overnightcultivated *E. coli* AN387 was washed and resuspended in buffer solution (0.05 MKH_2PO_4 and 0.05 M K_2HPO_4, pH 7.0) to ca. 10^9 colony-forming units per ml (cfu/ml).The cell suspension was pipetted onto a sterile petri dish which was illuminated by a visible-light source (ca.1.6 mW/cm^2) in the presence of the PdO/TiON fiber photocatalyst. At regular time intervals, 20 μL aliquots of the irradiated cell suspensions were withdrawn. After appropriate dilutions in buffer, aliquots of 2μL

together with 2.5 ml top agar were spread onto agar medium plates and incubated at 37 °C for 18-24 h. The number of viable cells in terms of colony forming units was counted. The *E. colirec*, a mutant strain AS224 was used for a comparative study following the same viability assay. The hypersensitivity ofAS224 mutants to DNA damage was confirmed with in-house UV irradiation prior to use of the bacteria. Through the chemical assay and several microscopic techniques (such as scanning electron microscopy (SEM), transmission electron microscopy (TEM), fluorescence microscopy, atomic force microscopy (AFM)), the cellular responses of *E. coli* tovisible light photocatalysis at different treatment intervals were characterized in detail.

Figure 2(a) shows a representativeSEM image of *E. coli* cells before photosterilization treatment. In this control sample, the surfaces of rod like bacteria are smooth and damage-free. It indicates that the cells are healthy before they are treated with PdO/TiON photocatalyst. However, after complete disinfection of the bacteria cells under visible-light illumination for 2 h in the presence of PdO/TiON photocatalyst, the morphologies of cells show drastic changes. First, flagella which are observed in untreated cells are completely missing in Figure 2(b) and (c) of treated cells. Second, in nearly every cell, the appearance of rumples and a high degree of disconfigurations are observed. Images in Figure 2(b) and (c) show that many *E. coli* cells are missing parts of the cell wall and the cell membrane or even material inside, so that deep 'holes' appear. These images obtained in two separate sets of experiments verify that photocatalysis causes oxidative damages on bacteria. It is interesting to note that after treatment for 30 min (with ~90% cell population "destroyed" as indicated by the viability assay), the cell morphology and its surface structure change little as shown in Figure 2(d). It indicates that at this disinfection stage, when bacteria cells have just lost their viability, the exterior damage in morphology has occurred; yet the damage is too subtle to be observed under SEM.

Figure 3(a) is a representative TEM image ofuntreated *E. coli* cells that have a fluffy boundary. The fluffy outer layer is considered to be the outer membrane of *E. coli* cell. It can benoted that after photocatalytic disinfection, the outer membrane is completely decomposed. In Figure 4(b)-(d) after treatment for 2 h, a noteworthy difference from the untreated sample is that every treated cell has lost its outer membrane,

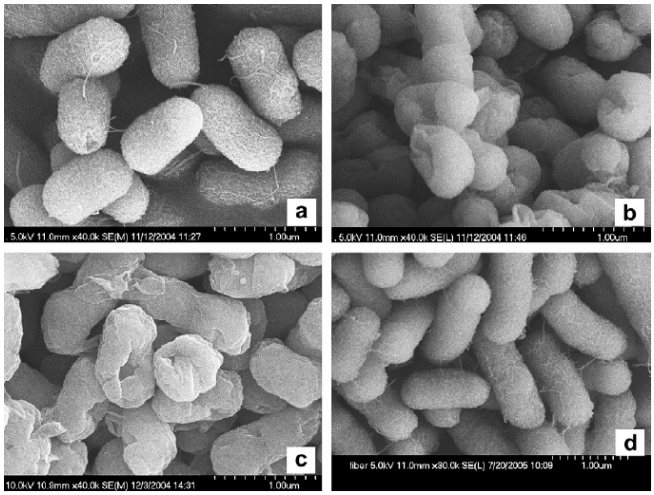

Figure 2: SEM images of *E. coli* cells (a) untreated; (b) and (c) after photocatalytic inactivation treatment for 2h; and, (d) after photocatalytic inactivation treatment for 30 min [50].

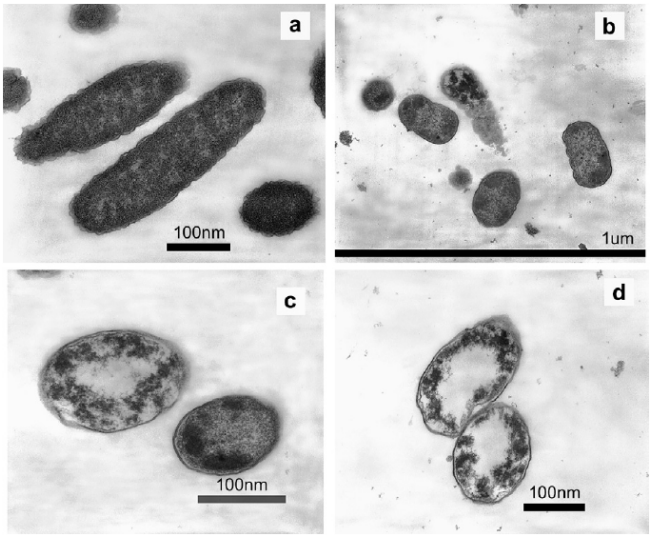

Figure 3: TEM images of *E. coli* (a) untreated; (b), (c), and (d) after photocatalytic inactivation treatment for 2h [50].

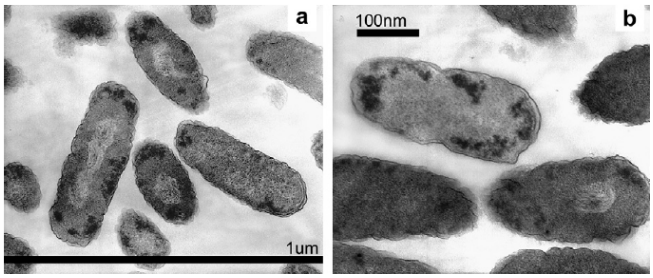

Figure 4: TEM images of *E. coli* cells after photocatalytic inactivation treatment for 30 min [50].

i.e., the fluffy boundary. Some treated cells show a clearly-cut edge, which indicates that the plasma membrane may have been exposed after theo uter membrane has decomposed. The other cells completely or partially lose this edge, which is a severely damaged stage with plasma membrane also gone. An extensively damaged 'ghost' cell is apparent in the center of Figure 4(b). There remains no more cell wall or cell membrane in this cell; instead, many dark granules appear.

TEM images also show remarkable interior damage of the cells after photocatalytic disinfection. Normal *E. coli* cells exhibit a homogeneous microstructure in Figure 3(a). This image shows that a healthy *E. coli* cell has a well-defined cell wall and a uniform interior material distribution, which corresponds to an inner zone full of proteins and DNA molecules. In contrast, dark mass aggregates appeared in the 2h well-treated cells in Figure 3(b)-(d). In some more severely compromised cells in Figure 3(c) and (d), white center regions are observed.

Figure 4 shows TEM images of an intermediate killing stage after treatment for 30 min. Many cells still have a fluffy outer boundary, similar to that in control cells. However, a remarkable material-light center tends to be formed in the *E. coli* cells. In Figure 4(a) some substances are visible within the material-light region, in contrast to the pure-white regions of Figure 3(c) and (d). These "struggling"

substances are coiled or twisted, like fingerprints. There are also some electron-dense granules/mass aggregates near the cell wall and membrane boundaries. In Figure 4(b), an *E. coli* cell is more severely damaged, as its outer membrane seems to be decomposed (lacking the fluffy edge) and its inner structure badly disturbed. A few individual cells appear less damaged, except for a few material-dense dark granules. Results indicate that the delicate cell membrane is subject to oxidative damage first by the very reactive hydroxyl radicals. The initial membrane damage is so subtle that it is not detectable in SEM and TEM until the damage advances to a greater level. But as soon as the cell's first line of defense (which is the cell wall and membrane) is broken, some interior substances (including the sensitive DNA molecules) are damaged almost immediately and readily observable in TEM.

Furthermore, in the previous works [51], TiONis also fabricated into both powder and thin film.Compared with TiON thin films, TiON powder photocatalysts offer theadvantages of high surface area, low cost, and suitability for large-scaleproduction. Among various synthesis methods for preparing TiON powders,sol-gel based processes [52,53] seem to have the most potential. However, a systematic study of the precursor ratio effect on thestructure, composition, and optical properties of sol-gel derived TiONnanoparticles [54] should be focused on.

Porous titanium oxide (TiO_2): Sol-gel synthesis

Research efforts in photo catalysis have dramatically expanded since the discovery of the photocatalytic properties of TiO_2 and the demonstration of its effectiveness to generate hydroxyl radicals in the presence of UV. TiO_2 photo catalysis is of particular interest because of its environmentally friendly features. The process can completely oxidize virtually all organic contaminants (nonselective) without addition of any other chemicals for the reaction and thus produce no harmful end products in most cases. Especially, TiO_2 photocatalysis forms no disinfection by-products unlike other chemical oxidation processes when sufficient time is allowed for organic mineralization. In general, the photo catalytic process has features of a green engineering process. Although various materials (oxides: TiO_2, ZnO, ZrO_2, CeO_2, SnO_2, Fe_2O_3, $SbrO_4$; sulfides: CdS, ZnS) have been used for photo catalysis, generallyTiO_2 is the most promising photo catalyst, considering its energy efficiency, durability, photo stability, water insolubility and nontoxicity [55-60].

Among various synthesis methods of TiO_2, sol-gel technology, which involves the formation of solid inorganic materials from liquid molecular precursors, is popular for the fabrication of TiO_2 inorganic materials with engineered properties because of (i) room temperature wet chemistry based synthesis, (ii) wide-range selection of precursors and support materials, (iii) precise control of the properties of TiO_2 at the molecular level, and (iv) easy doping with other metals or nonmetals in TiO_2 matrix. During the sol-gel synthesis of TiO_2, surfactant molecules as a pore directing agent in the TiO_2 inorganic matrix are introduced, as demonstrated in Figure 5 [61]. Under certain conditions, surfactants are known to self-assemble into various structures (micellar, hexagonal, lamellar) in a water-rich environment [62]. For example, when liquid-phase TiO_2 precursors are added in the surfactant micellar aqueous solution, the TiO_2 precursors are hydrolyzed and condense to form a solid TiO_2 inorganic network around the micelles, forming a surfactant organic/TiO_2 inorganic composite. During thermal treatment, the surfactant templates are pyrolyzed, leaving the TiO_2 inorganic matrix

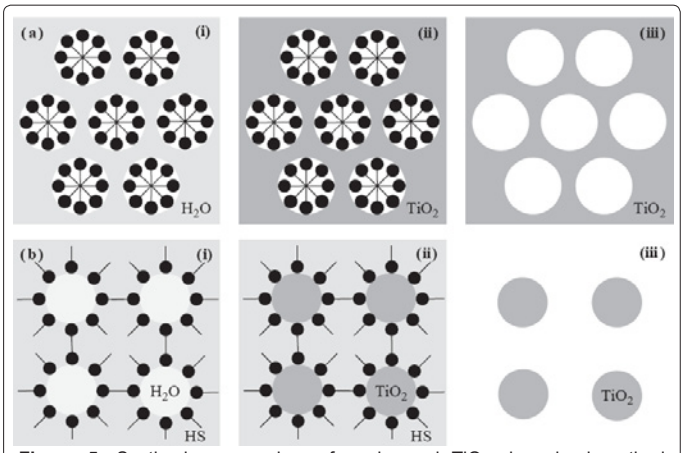

Figure 5: Synthesis approaches of engineered TiO_2 via sol-gel method employing surfactant self assembly as (a)aporetemplate and (b)particle growth template (a)Synthesis of TiO_2 with mesoporous inorganic network: (i)surfactant molecules are self-organized in water-rich environment forming surfact and the head group outside towards water molecules and its tail group inside free from water, (ii)titanium alkoxide precursor ishydrolyzed and condensed to form TiO_2 inorganic network around the self-assembled surfactant, forming a surfactant organic template-embedded TiO_2 inorganic matrix and (iii)porousTiO_2 inorganic network is formed after removal of the organic template by thermal treatment or organic extraction. (b)Synthesis of TiO_2 nanoparticles: (i)surfactant molecules are self-organized in water-poor environment (bulk hydrophobic solvent(HS) with small portion of water) forming surfactant head group inside towards water molecules and its tail group outside towards HS, (ii)titanium alkoxide precursor is hydrolyzed and condensed to form TiO_2 in organic network in the waterphase, inside of self-assembled surfactant, forming TiO_2 inorganic core/surfactant organic shell structure and (iii)well-defined TiO_2 nanoparticles are formed after removal of the organic template [61].

with a porous structure. In the case of water-poor conditions, the situation is reversed toform reverse micellar structures, then TiO_2 inorganic core/surfactant organic composites, and finally well-defined TiO_2 nanoparticles [63].

Adsorption of chemicals to TiO_2

It is well known that someb of the electron and hole pairs migrating to the surface get involved in redox reactions even during their short lifetime (on the order of nanoseconds). Titanium (IV) is reduced to titanium (III), which is finally transformed totitanium(IV) combined with superoxide radical anions if electron acceptors such as oxygen are available on the surface listed as follows:

$$Ti^{IV} + e^- \rightarrow Ti^{III}$$

$$Ti^{III} + O_2 \rightarrow Ti^{IV} - O_2^{\bullet -}$$

At the same time, the generated holes are utilized for the generation of hydroxyl radicals and direct oxidation of organics, R (shown as follows) or they can be combined with the electron from a donor species, depending on the reaction mechanism:

$$Ti^{IV} - OH^- + h^+ \rightarrow Ti^{IV} - OH^{\bullet}$$

$$Ti^{IV} - H_2O + h^+ \rightarrow Ti^{IV} - OH^{\bullet} + H^+$$

$$R_{ads} + h^+ \rightarrow R_{ads}^+$$

Because of the short lifetime of photo carriers, the prerequisite for above-mentioned reactions is the adsorption of substances such as water and organic molecules on the TiO_2 surface and lattice oxygen (O_L^{2-}) shown as follows. This facilitates the redox reaction at the interface of TiO_2 solid and the water:

$$O_L^{2-} + Ti^{IV} + H_2O \rightarrow O_L H^- + Ti^{IV} - OH^-$$
$$Ti^{IV} + H_2O \rightarrow Ti^{IV} - H_2O$$
$$TiO_2 + R \rightarrow R_{ads}$$

Radical attack on organics

The hydroxyl radicals, the primary oxidizing species in the photo catalytic system, initiate chain reactions leading to the generation of other radicals and subsequently oxidation of organics [63]. Even though it is not necessary for the reaction that hydroxyl radicals and organics are adsorbed at the TiO_2 sites, the adsorbed forms are much more helpful to increase the overall reactivity, compared to those free from TiO_2 sites:

$$Ti^{IV} - OH^{\bullet} + R_{ads} \rightarrow Ti^{IV} + R'_{ads}$$
$$Ti^{IV} - OH^{\bullet} + R \rightarrow Ti^{IV} + R'$$
$$^{\bullet}OH + R_{ads} \rightarrow R'_{ads}$$
$$^{\bullet}OH + R \rightarrow R'$$

Other radicals and oxidants ($HO_2^{\bullet}$, H_2O_2) are also generated and are involved in redox reactions to decompose organic contaminants in water:

$$e^- + Ti^{IV} - O_2^{\bullet -} + 2H^+ \rightarrow Ti^{IV} + H_2O_2$$
$$Ti^{IV} - O_2^{\bullet -} + H^+ \rightarrow Ti^{IV} + HO_2^{\bullet}$$
$$H_2O_2 + {}^{\bullet}OH \rightarrow H_2O + HO_2^{\bullet}$$

After the photo excitation process and the generation of reactive species, a series of reactions lead to complete mineralization of the parent compound. These reactions include hydroxyl radical attack, hydroxylation (e.g., $^{\bullet}OH$ addition, reaction with O_2, and elimination of ($HOO^{\bullet}$), dihydroxylation, hydration, hydrogen abstraction, deprotonation, decarboxylation and one-electron transfer reactions [64].

In addition, polymer–inorganic porous composite membranes incorporating bimetallic (Ni/Fe, Pd/Fe) [73-77] and zero-valent iron [78-80] nanoparticles have been developed and applied to the reductive degradation of halogenated organic solvents.

Nanoparticles can also be introduced as components of polyelectrolyte multilayer films (PMFs). Importantly, when supported by a porous membrane, PMFs are known to have water permeabilities and ion rejections typical for nanofiltration membranes. The possibility to control the composition of the PMF in terms of its polymeric constituents and nanoparticles fillers and to regulate PMF's separation properties presents unique opportunities for the design of nanoparticle-enabled membranes [81-83].

Metal-polymer nanocomposite membranes can be prepared by the *in situ* reduction of unbound ionic precursors in the process of phase inversion, such as silver-polymer membranes were synthesized by reducing ionic silver chemically, by ultraviolet irradiation, or by heat [84-86]. Also, two silver incorporation approaches were adapted for NP-Ag-DMF (dimethylformamide). In the first approach, Ag nanoparticles were synthesized *ex situ* and were added to the casting solutionas Ag-DMF organosol. The organosol was prepared by adding $AgNO_3$ to DMF(reducing agent) and heating the solution under intense stirring conditions [87].The second approach involved an in situ reduction of ionic Ag + by DMF in the membrane casting mixture. In this case, $AgNO_3$ was first dissolved in DMF at room temperature to minimize Ag reduction.

Nanocomposite membranes

Nanocomposite membranes above-mentioned exhibit one to three times the water permeability with the same rejection as commercial reverse osmosis (RO) membranes, and can be imparted with anti-microbial and photo-reactive functionality.

Since Maxwell conceived the ideal membrane [88], membrane-based water purification processes are now among the most important and versatile technologies for conventional drinking water production, wastewater treatment, ultrapure water production, desalination, and water reuse.

Commercially available membrane processes for water purification include electrodialysis (ED), electro-deionization (EDI), reverse osmosis (RO), nanofiltration, ultrafiltration and microfiltration (MF). Nanofiltration, ED and EDI find some use in demineralization, softening, and organic separations, but RO and MF membranes are the workhorse technologies for desalination and water reuse. Other membrane based processes such as forward osmosis, membrane distillation, and pervaporation are emerging, but have found limited application in practice.

In principle, intrinsic advantages of membrane processes include continuous, chemical-free operation, low energy consumption, easy scale-up and hybridizationwith other processes, high process-intensity (i.e., small land area per unitvolume of water processed), and highly automated process control. General disadvantages of membrane processes are short membrane lifetime, limitedchemical selectivity, concentration polarization, and membrane fouling [88]. Polarization and fouling of RO membranes require extensive physical and chemical feed water pretreatment (i.e., filtration, acidification, antiscalant addition, disinfection), low flux operation, extensive chemical cleaning, and frequent operator intervention. Reverse osmosis processes further suffer from high intrinsic energy consumption, environmental issues associated with feed water intake and brine discharge, and the need for chemical conditioning of product water.

Nanotechnology promises to dramatically enhance many water purification technologies such as adsorption, ion exchange, oxidation, reduction, filtration, membranes, and disinfection processes [89]. However, one of the key issues related to nanotechnology is the question of how to apply it. Specifically, it isnot clear how to interface nanoparticles with contaminants. At present, many expensive nanoparticles cannot be added to water like commodity chemicals and some nanoparticles could present new hazards to human health and theenvironment [90]. Thus, additional separation processes are required recover nanomaterials for risk avoidance and reuse. A promising approach is to immobilize nanomaterials on or within a solid matrix, such as a membrane. The resulting membrane may exhibit improved separation performance, chemical, thermal, or mechanical stability, interfacial properties, or advancedfunctionality depending on the nanomaterial selected.

Inorganic–organic nanocomposite membranes

In general, nanocomposite materials are created by introducing nanoparticulate materials (the "filler") into a macroscopic sample material (the "matrix") [91]. The resulting nanocomposite material may exhibit drastically enhanced properties such as mechanical properties (e.g., strength, modulus, and dimensional stability);

chemical and thermal stability; permeability for gases, water, and hydrocarbons; electrical and thermal conductivity; surface properties, optical properties, or dielectric properties. For example, dispersing molecular sieve nanoparticles into polymers canproduce mixed matrix membrane materials with improved gas mixture perm selectivity [92].

In the literature [93], the synthesis and characterization of zeolite-polyamidethin film nanocomposite (TFN) membranes formed by interfacial polymerization are expressed. The general approach to TFN membrane formation is similar to that of traditional polyamide thin film composite (TFC) membranes, but nanoparticles are dispersed in the initiator solution prior to interfacial polymerization as depicted schematically in Figure 6. Figure 6 shows that the embedded molecular sieve nanoparticles throughout the polyamideth in film layer of an interfacial composite RO membrane. Synthesized NaA zeolite nanoparticles, characterized by a super-hydrophilic and negatively charged three-dimensional molecular sieve pore network, are used as the dispersed nanophase. Thin film nanocomposite membranes offer new degrees of freedom in designing NF and RO membranes because the nanoparticle and polymer phases can be independently designed to impart a wide array of separation performance and novel functionality. Where, the zeolite nanoparticles (NaA-type) were synthesized from the Na_2O-SiO_2-Al_2O_3-H_2O system with the use of an organic template (tetramethyl ammonium hydroxide) by a hydrothermal reaction. The as-synthesized zeolite A nanoparticles are porefilled because the presence of the template inside the zeolite pore structures. Pore-opened zeolite nanoparticles were obtained from the pore-filled particles by removing the template by calcinations, assisted by a polymer network as designed as atemporary barrier to prevent nanoparticle aggregation during the calcination process.

Both TFC and TFN membranes were hand-cast on preformed polysulfone ultrafiltration (UF) membranes (provided by KRICT, Korea) through interfacial polymerization. A UF membrane taped to a glass plate was placed in an aqueous solution of 2% (w/v) *m*-phenylenediamine(MPD, >99%,Sigma–Aldrich) for approximately 2 min, and MPD soaked support membranes were then placed on a rubber sheet and rolled with a rubber roller to remove excess solution. The MPDsaturated UF membrane was then immersed in a solution of 0.1% (w/v) trimesoyl chloride (TMC, 98%, Sigma–Aldrich) inhexane. After 1 min of reaction, the TMC solution waspoured off and the resulting membranes were rinsed with an aqueous solution of 0.2% (w/v) sodium carbonate (Na_2CO_3, HPLC grade, Fisher Scientific). Nanocomposite membranes were made by dispersing 0.004-0.4% (w/v) of synthesized zeolite A nanoparticles in the hexane-TMC solution. Nanoparticle dispersion was obtained by ultrasonication for 1 h at room temperature immediately prior to interfacial polymerization. Figure 7 shows the morphology of the final synthesized zeolite nanoparticles.

Figure 8(a)-(f) are SEM images of synthesized TFC andTFN membrane surfaces. The five TFN membranes depicted in Figure 8(b)-(f) were synthesized with increasing nanoparticles loadings. At zero and low nanoparticle loadings, depicted in Figure 8(a) and (b), surfaces of both TFC and TFN membranesexhibit the familiar “hill and valley” structure of polyamide RO membranes. At higher zeolite loadings, Figure 8(c)-(f), but particularly Figure 8(f), zeolite nanoparticles are visible on themembrane surface. Three white circles drawn in Figure 8(f) around features are believed to be zeolite nanoparticles because of their more “cubic” shape, which is consistent with the morphology of zeolite A nanoparticles. Also, EDX analysis confirms nanoparticle presence at discrete locations within the film layer and at the interface. Results show that the formation of zeolite-polyamide nanocomposite thin films by interfacial polymerization are resulted in reverse osmosis membranes with dramatically improved permeability and interfacial properties when compared to similarly formed pure polyamide thin films. This new concept combines important properties of conventional membrane polymers(flexibility, ease of manufacture, high packing-density modules)with the unique functionality of molecular sieves (tunable hydrophilicity, charge density, pore structure, and antimicrobial capability along with better chemical, thermal, and mechanical stability).Water molecules appear to flow preferentially through super-hydrophilic, molecular sieve nanoparticle pores, while solute rejection remains comparable to pure polyamide membranes. Pendergast et al. [94] assess the compaction behavior of hand-cast nanocomposite supported polyamide composite membranes relative to polysulfone supported olyamide composite membranes to help understand and control irreversible, internal fouling of RO membranes by physical compaction. Support membrane preparation was prepared with addition of N-methyl pyrrolidone (NMP) (Acros Organics, Morris Plains, New Jersey, USA) to a mass of transparent polysulfone

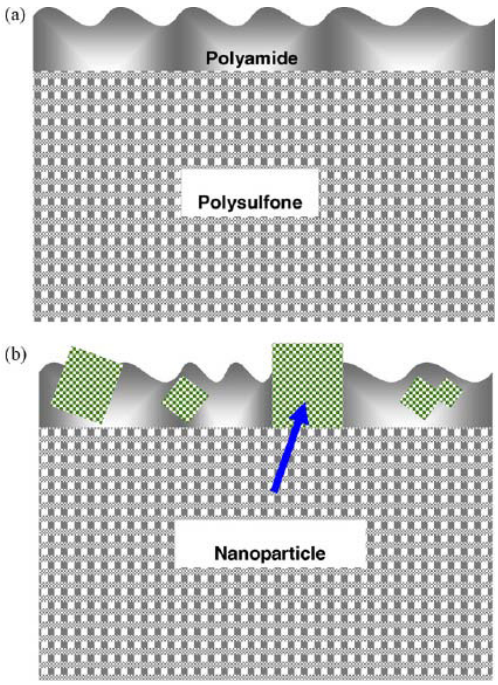

Figure 6: Conceptual illustration of (a) TFC and (b) TFN membrane structures [93].

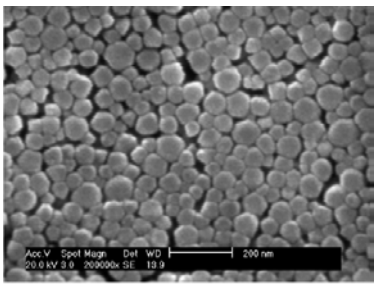

Figure 7: Properties of synthesized zeolite nanoparticles by SEM [93].

beads (Mn-26,000 from Aldrich, St. Louis, Missouri, USA) in airtight glass bottles. For nanocomposite membranes, nanoparticles were dispersed in the NMP before additionto the polysulfone beads. The solution was then agitated for several hours until complete dissolution was achieved. This prepared casting solution was spread via knife-edge over a polyester non-woven fabric (Nano H_2O Inc., Los Angeles, California, USA) previously taped to aglass plate. After spreading the casting solution, the glass plate was immediately immersed in a bath of 18 μΩ laboratory deionized water maintained at 20±2°C. After several minutes, the non-woven support fabric with polysulfone membrane was separated from the glass plate. The membrane was then washed thoroughly with deionized water and stored in a refrigerator at 5 °C. Meanwhile, polyamide thin films were formed atop polysulfone and polysulfone-nanocomposite supports. The support membrane was immersed in a 2.0 wt.% aqueous solution of *m*-phenylenediamine (1,3-diaminobenzene,Sigma-Aldrich, Milwaukee, Wisconsin, USA) for 15 s. The excess MPD solution was then removed from the skin surface of the supportmembrane via an air knife. The membrane was then immersed into asolution of 0.1 wt. % trimesoyl chloride (1,3,5-tricarbonyl chloride, Sigma-Aldrich, Milwaukee, Wisconsin, USA) in a proprietary isoparrafin(Exxon Mobil Isopar G, Gallade Chemical, Inc., Santa Ana, California) for 15 s initiating polymerization. The resulting composite membranes were heat cured for 10 min at 82 °C, washed thoroughly with deionized water, and stored in deionized water until performance testing. Subsequently, membrane samples were placed into the crossflow membranemodules and compacted with a 10 Mm NaCl feed solution at pressuresof 1700 and 3400 kPa (250 and 500 psi). The compaction tests continued until a steady-state flux was obtained for both membranes (typically, 16-20 h), at which point the membranes were removedand stored in a desiccator for subsequent characterization. Observed permeate water flow rate was recorded every 30 min. Figures 9-15 show the cross-sectional thicknesses of uncompacted (as-cast) and compacted RO membranes analyzed by SEM. It indicates that membranes containing nanoparticles undergo less compaction, while the pure polysulfone membrane experiences a drastic change in thickness and support structure. In general, TFN supported membranes undergo less compaction, and all the membranes containing nanoparticles appear to maintain their uncompacted porous structure following compaction, while pure polysulfone supported membrane (TFC) macrovoid morphology changes after compaction. Hence, the addition of inorganic nanoparticles increases the mechanical stability and, therefore, decreases physical compaction of the nanocomposite supported membranes. The performance advantage of nanocomposite supported membranes is greater at higher applied pressure, and nanocomposite-supported RO membranes represent one potential approach to mitigate internal, irreversible fouling due to membrane compaction, particularly in high-pressure applications like brackish and ocean water desalination.

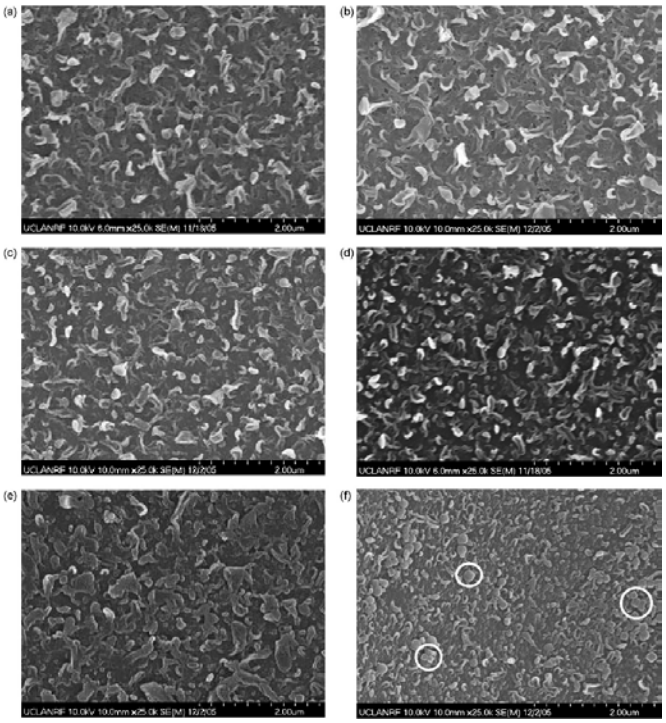

Figure 8: SEM images of (a) TFC and (b-f) TFN membrane surfaces. Nanoparticle loadings are (a) 0.0%, (b) 0.004%, (c) 0.01%, (d) 0.04%, (e) 0.1%, and (f) 0.4%(w/v) [93].

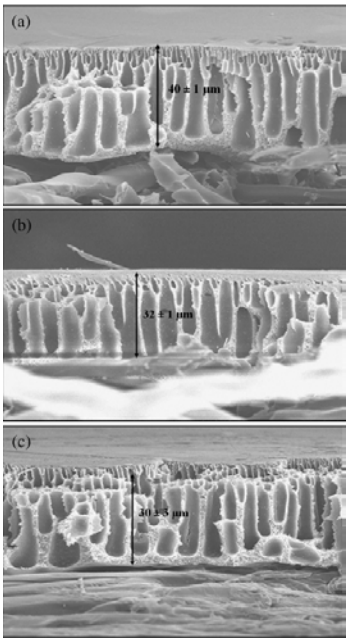

Figure 9: SEM images of TFC (a) uncompacted and compacted at (b) 1724 and(c) 3448 kPa [94].

Fathizadeh et al. [95] also used the nano-NaX zeolite synthesized via the hydrothermal method to investigate the effect of nano-NaX zeolite dispersed in the zeolite-polyamide thin film nanocomposite on the membrane performance, the matrix structure, film thickness and surface hydrophilicitity.

Results show that nano-NaX zeolite increases physical and chemical stability properties. Also, the surface properties such as contact angle, RMS roughness and interfacial free energy as well as water permeability improved by increasing the content of nano-NaX in the polyamide structure. An enhancement in the concentration of MPD and TMC monomers lead to production of TFN membrane with high water permeability and low solute rejection. The TFN membrane with high concentration of TMC (0.15%, w/v), MPD (3%, w/v) and nano-NaX zeolite (0.2%, w/v) (B4 sample) has the highest waterflux and the lowest salt rejection. The A4 TFN membrane demonstrates

a good separation efficiency, productivity flux and thermal stability between the TFN and TFC membranes.

Biomimetic membranes

Biomimetic membranes are designed to mimic the highly selective transport of water and solutes across biological membranes [96-99]. The general approach to forming biomimetic membranes is to incorporate active transport proteins (isolated from cell cultures) within a vesicular or planar lipid bilayer or a more stable synthetic analog. Liu et al. [100]

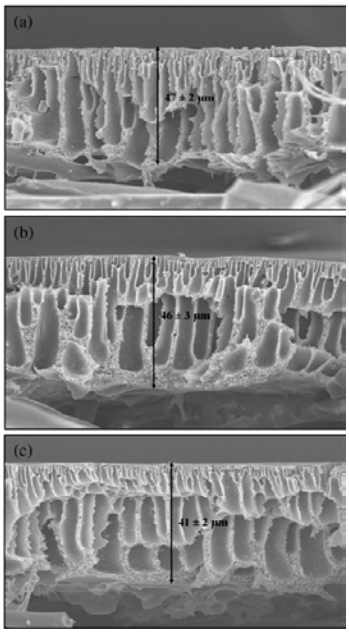

Figure 10: SEM images of ST50-TFC (a) uncompacted and compacted at (b) 1724 and(c) 3448 kPa [94].

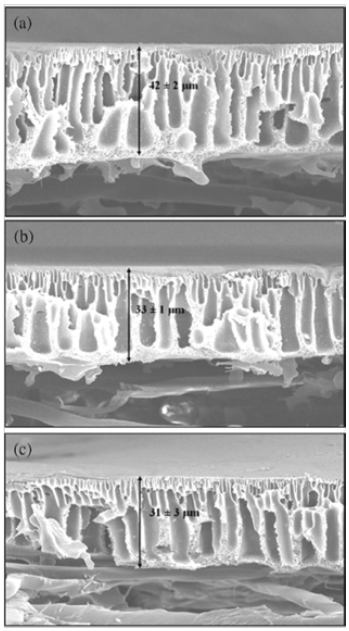

Figure 11: SEM images of ST20L-TFC (a) uncompacted and compacted at (b) 1724 and(c) 3448 kPa [94].

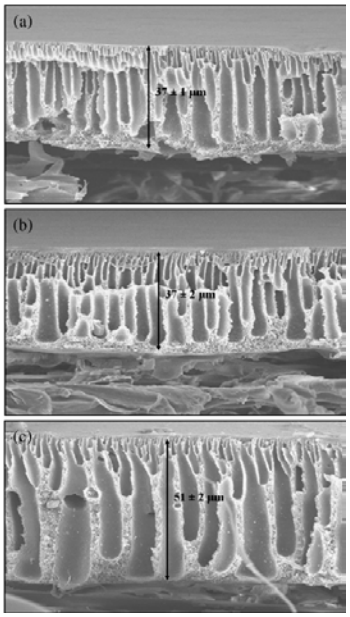

Figure 12: SEM images of STZL-TFC (a) uncompacted and compacted at (b) 1724 and(c) 3448 kPa [94].

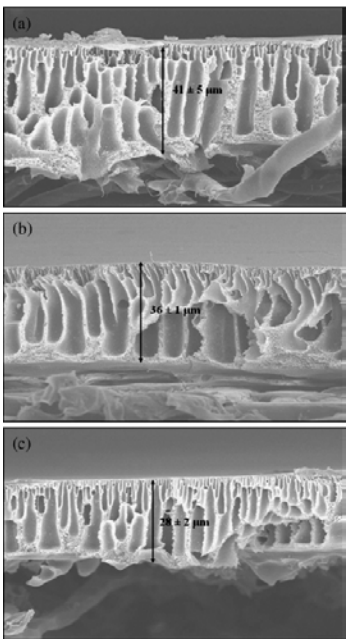

Figure 13: SEM images of MP1040-TFC (a) uncompacted and compacted at (b) 1724 and(c) 3448 kPa [94].

developed a novel biomimetic absorbent containing the lipid triolein for removing persistent organic pollutants (POPs) from water in 2006 using the concept of bioaccumulation. A cellulose acetate (CA) polymer was chosen for preparing hybrid materials because it can be easily molded into different forms such as membranes, fibers and spheres. Furthermore, its hydrophilicity improves the accessibility of aqueous solutions to the surface of the film. The absorbent was prepared by embedding triolein into cellulose acetate (CA) spheres and the temperature ranges of the CA solution and liquid olefin were kept at

30-35°C and 15-20°C respectively. Finally, composite absorbents were washed with distilled water to remove all soluble impurities. It shows that the biomimetic absorbent can be prepared with these pollution-free and environmentally friendly raw materials and the spherical absorbent is easy to use in water treatment processes.

Figure 16 presents SEM micrographs of the absorbent cross sections containing no triolein and those containing 2.0 % (w/w) triolein. Figures 16(a) and (c) show that both absorbents present a very thin layer from the top surface. Triolein dropletscannot be seen in the layer that should be the CA membrane.This could be explained by the aggregating rate of CA into theair being faster than that of triolein. In addition, triolein loadingis likely to affect the process of formation of the CA membrane.A careful inspection of the images of Figure 16(a) and (c) reveals that the layer of the CA-triolein absorbent is thinner than that of CA. The thickness of the CA and CA-triolein absorbentlayers is about 10 mm and 5 mm, respectively.

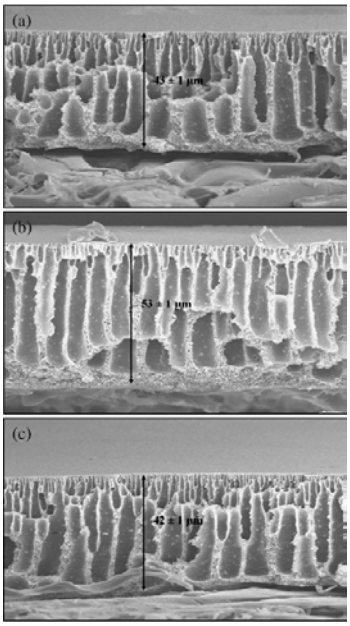

Figure 14: SEM images of LTA-TFC (a) uncompacted and compacted at (b) 1724 and(c) 3448 kPa [94].

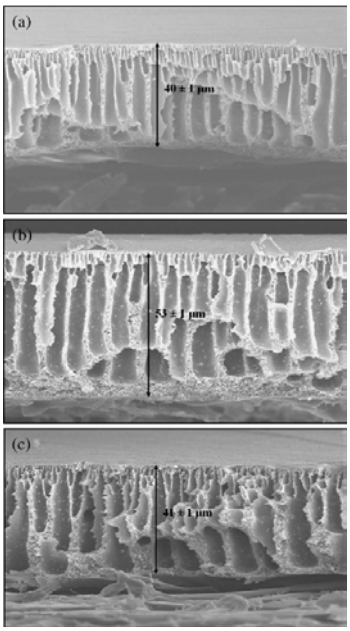

Figure 15: SEM images of OMLTA-TFC (a) uncompacted and compacted at (b) 1724 and(c) 3448 kPa [94].

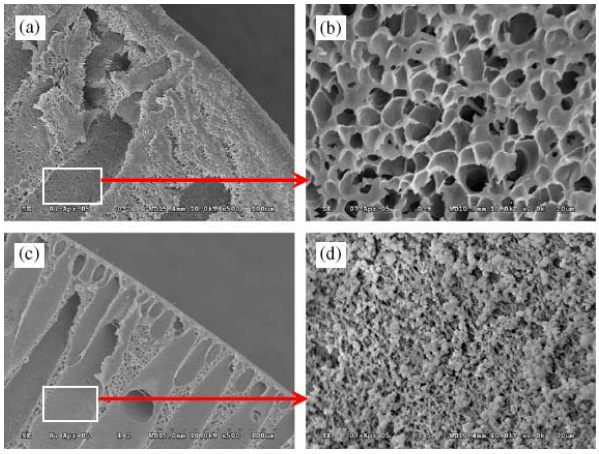

Figure 16: SEM micrographs of cross-sections of CA and CAetriolein absorbents.(a) CA absorbent (×500), (b) CA absorbent (×2000), (c) CA-triolein absorbentcontaining 2.0% (w/w) triolein (×500), and (d) CA-triolein absorbent containing 2.0% (w/w) triolein (×2000) [100].

Figures 16(b) and (d) are the partially amplified images of Figure 16(a) and (c), respectively. Itillustratesthat CA formed mesh structures. The image of the CA-triolein absorbent shows fewer pores and triolein droplets that have been embedded into the hole formed by the CA fiber. Triolein is wrapped in the thin CA polymer, and constitute a significant fraction of the lipid pool in the absorbent. This biomimetic absorbent should be most effective in its capacity to accumulate lipophilic substances. In addition, the thin CA polymer canprevent triolein leakage. Results reveal a higher affinity of CA and CA-triolein absorbents for the most hydrophobic and less polar compounds of the group. The role of triolein is probably similar to that of an organic solvent in a liquid-liquid extraction. The distribution of a neutral organic compound between the biomimetic absorbent and water can be correlated with the octanol-water partition coefficient. It also indicates that triolein is effectively embedded into CA spheres and that a thin film of CA surface layer containing no triolein is formed, thus ensuring that virtually no triolein leaks out through the CA membrane. The absorbent are promising for the removal of non-polar compounds. The CA-trioleinabsorbent can efficiently and quickly accumulate hydrophobic POPs from water. Lower residual concentrations of selectedPOPs are obtained by the CA-triolein absorbent in comparison with the CA absorbent.

Moreover, James et al. [101] propose an optrode based on the use of ion imprinted polymers (IIPs) particles prepared via chemical immobilization afterthe formation of mixed ligand complex, uranium-4-vinylphenylazo-2-naphthol (VPAN)-4-vinyl pyridine (VP) and then polymerization with matrix forming monomers. The predetermined selectivity, operational stability ofthe sensing material (IIP) is more advantageous compared to conventional optical sensors.

Membranes incorporating bacterial Aquaporin *Z* proteins have been reported to show superior water transport efficiency relative to

conventional RO membranes. Aquaporins were incorporated into the walls of self-assembled polymer vesicles constituted of tri-block co-polymer, poly (2-methyl-2-oxazoline)-blockpoly (dimethylsiloxane)-block-poly (2-methyl-2-oxazoline). An initial permeability test was carried out on the aquaporin-triblock polymer vesicles by stopped-flow light-scattering experiments. The results reported at least an order of magnitude improvement in permeability compared to commercially available TFC RO membranes. Although a salt separation test has yet to be reported,extremely high salt rejection is expected from aquaporins sincetheir functional biological performance is to only allow the passageof water molecules. Hence, there is an ideal opportunity forthe production of ultrapure water. These studies haveso far been limited to investigating water permeability propertiesacross a barrier layer composed of aquaporins and triblock polymers [102].

Carbon nanotubes (CNTs) membranes

It is distinct that the availability of safe, clean, and inexpensive water has emerged as an issue that defines global problem in the twenty-first century. Water short ages are some of the root causes of societal disruptions such as epidemics, environmental disasters, tribal and ethnic conflicts, growth shortfalls, and even countrywide political destabilization. Membrane-based filtration is the current leading energy-efficient technology for cleanup and desalination of brackish water, recycled water, and seawater. Membrane-based filtration offers other advantages as filtration through the tight membrane pores can also remove dangerous impurities, such as As, as well as toxic large organic compounds. Factors that limit the efficiency of the membrane purification technologies include the membrane resistance to the flow, membrane fouling and membrane imperfections that lead to incomplete rejection or to a drop in the membrane rejection properties over time. The technological developments and high-efficiency energy recovery systems in particular have pushed the current efficiency of reverse osmosis (RO) membranes to a very impressive 4 kWh/m^3 [103,104]; However, this number is still well above the theoretical minimum energy cost of 0.97 kWh/m^3 for 50 percent recovery [105,106]. To move further, the transformative membrane technologies that utilize fundamentally new transport and filtration mechanisms for drastic gains in transport efficiency need to be developed.

Carbon Nanotubes (CNTs) [107,108] are unique nanosystems with extraordinary mechanical and electronic properties, which derive from their unusual molecular structure. An ideal carbon nanotube can be thought of as a single graphite layer (graphene sheet), rolled up to make a seamless hollow cylinder. These cylinders can be tens of microns long, with diameters as small as 0.7 nanometers and are closed at both ends by fullerene-like caps. CNTs having wall thickness of one carbon sheet are named single-wall carbon nanotubes (SWCNTs). In consequence of the Vander Waals interactions between nanotubes, they often aggregate in large ropes: ordered arrays of SWCNTs arranged on a triangular lattice. SWCNTs can be considered as the building blocks of multi-wall carbon nanotubes (MWCNTs), which consist of a coaxial array of SWCNTs with increasing diameter. MWCNTs are also usually long many microns, with the external diameter that ranges from two to several tens of nanometers, providing very high aspect ratio structures, as shown in Figure 17 [108].

By now the CNT has firmly established itself as the iconic molecule of nanoscience [109-113]. Several methods of CNT production currently exist. In the laboratory environment, catalytic chemical vapor deposition (CVD) is preferred over other methods such as arc discharge and laser ablation because it produces higher quality CNTs. CVD

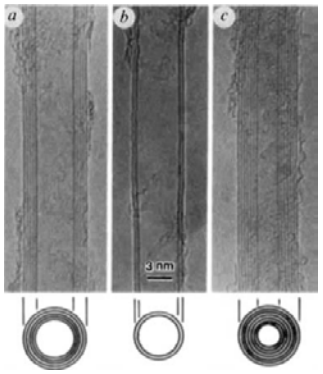

Figure 17: Electron micrographs of microtubules of graphitic carbon [108].

reactors can produce individual isolated nanotubes as well as densely packed vertically aligned arrays. Unfortunately, the ultimate goal of the CNTs synthesis—producing a uniform population of nanotubes with a given chirality—still remains elusive. Several studies indicated that the size of the catalyst particle during the growth stage determines the size of the CNT to less than 10 percent; yet efforts to control the size of the CNTs with greater precision have been largely unsuccessful. Thus, synthesizing a vertically aligned CNT array with a narrow distribution of sizes still remainsa difficult endeavor requiring considerable process development and optimization efforts [114-116].

In the last decade, the unique geometry and internal structure of carbon nanotubes (CNTs)give rise to the newly discovered phenomena of the ultraefficient transport of water through these ultra-narrow molecular pipes. Water transport in nanometer-size nanotube pores is orders of magnitude faster than transportin other pores of comparable size [111,112,115-118].

Simulation/dynamic analysis on water transport in carbon nanotubes (CNTs)

It is extremely important to understand the mechanism that hydrophilic liquids, especially water, enter and fill very narrow and hydrophobic CNTs. If the water does enter the CNTs, what influence does crucial confinement have on the water structure and properties, such as how these changes in structure influence the rate, efficiency, and selectivity of the transport of liquids and gases through the CNTs. As the traditional method, molecular dynamics (MD) simulations or dynamic analysis will provide the exact answers to these questions.

It is well known that confined matter on the nanometer scale differs significantly from bulk matter. The special properties of confined water can influence molecular transport inside membrane pores. Confinement of water can be reached by limiting the size of water agglomerates in one, two, or three dimensions. In an infinite ice crystal each water molecule, complying with the "bulk ice rule" [119], is tetrahedrally coordinated, simultaneously donating and accepting two hydrogen atoms, forming a hydrogen bonded network. However this arrangement is disrupted in agglomerates of crystalline water of finite sizes, leading to a variety of shapes for small water clusters with different types of OH groups ranging from bulk-like to essentially free OH groups. This diversity can be readily detected by means of vibrational spectroscopy that provides one of the most insightful means for OH characterization. In order to express the details of water phase inside single-walled carbon nanotubes (SWCNTs), Byl et al. [120] studied the unusual hydrogen bonding in water-filled carbon nanotubes.

They had performed classical molecular simulations (MD) for water confined in SWNTs and also carried out quantum mechanical density functional theory (DFT) calculations for water in ring structures in vacuum and inside a SWNT. Where: classical molecular simulations were used to identify structural, energetic, and vibrational properties of water in SWNTs and in the bulk phase at low temperatures. The average energies for water confined in armchair (8, 8), (9,9), (10, 10), and (11, 11) SWNTs are shown in Figure 18. Atlow temperatures water forms stacked ring structures in all of the nanotubes considered. See, for example, the water structure in a (10, 10) nanotube shown in Figure 19. The number of water molecules in a ring depends primarily on the diameter of then anotube. However, the (8, 8) and (10, 10) nanotubes can support different polymorphs. Five- and four-membered rings are observed in the (8, 8) nanotube, while the (10, 10) nanotube can have both eight- and seven-membered rings, as shown in Figure 18. Order-to-disorder structural transitions, indicated by rapid rises in the potential energy with temperature (Figure 18), occur for water confined in (10, 10) and (11, 11) SWNTs; the water remains well-ordered in the smaller diameter nanotubes, even at 298 K. The nanotubes were filled at room temperature for computational efficiency.

Results show that H_2O molecules confined inside of SWNTs form ring structures that involve hydrogen bonds of two types. Hydrogen bonds within the ring structure exhibit frequencies like those found in bulk H_2O and O-OH angles of near 5°. Hydrogen bonds formed between neighboring rings exhibit an unusual stretching frequency at 3507 cm^{-1} and are associated with larger O-OH angles near 17°. The strained angles and unusual IR mode are a direct result of the confinement-induced stacked ring structures, which would not be stable in the bulk. It is possible that water in other confined environments will exhibit similar distinct stretching frequencies, showing that IR spectroscopy, coupled with atomistic modeling, is proving to be a powerful tool for probing the structure and energetics of confined water.

Because open-ended CNT membranes, which are formed by filling the interstitial region between 1 and 10 nm diameter CNTs with a non-porous matrix material, have been proposed as next-generation desalination, results from molecular dynamics (MD) simulations suggest that flow enhancement in CNTs is caused by liquid slip at the water/carbon boundary and confinement-related changes in the liquid viscosity [121-123]. Thomas et al. [124,125] used MD simulation to study water flow in CNTs with diameters between 4.99 nm and 1.66 nm. It is predicted the variation in flow enhancement with CNT diameter and identified how it is related to the water viscosity and the water/CNT

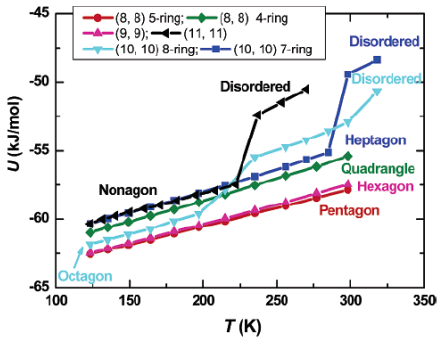

Figure 18: Average energy for water confined in (8, 8), (9, 9), (10, 10),and (11, 11) SWNTs at temperatures ranging from 123 to 318 K fromparallel tempering NVT Monte Carlo simulations.

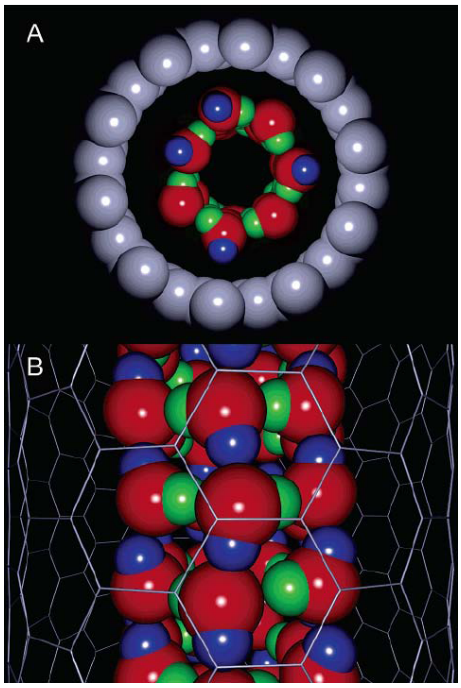

Figure 19: Snapshot from a molecular simulation of water adsorbed insidea (10, 10) SWNT at 123 K forming heptagon rings: (A) end view and (B)side view. Red spheres represent oxygen atoms, blue spheres are hydrogensthat are hydrogen-bonded to adjacent rings (inter-ring), and green spheresare hydrogens involved in intra-ring hydrogen bonds. The lines in part Brepresent the carbon-carbon bonds of the SWNT.

slip length. Results show that liquid flow through CNTs with diameters as small as 1.66 nm can be described using the slip modified Poiseuille relation. In addition, predictions from MD simulations indicate that (i) a continuum description of water flow is appropriate inside CNTs larger than 1.66 nm, (ii) diameter-related changes to the viscosity and slip length must be considered when modeling liquid flow, and (iii) the flow enhancement factor decreases monotonically with increasing diameter for smooth walled tubes. The variation in flow enhancement predicted using MD is qualitatively consistent with the majority of the experimental data. Since the MD simulations considered flow though atomically smooth and defect-free CNTs, discrepancies between simulation and experiment are likely caused by differences in the structure and/or chemistry of the carbon surface.

Furthermore, since the properties of nanotubes conveying fluids are highly sensitive to the vibrational characteristics, investigation of CNTs'dynamical properties is very important. Hashemnia et al. [126] described the dynamical analysis of carbon nanotubes conveying water considering carbon–water bond potential energy and nonlocal effects. Where: it was assumed that fluid media was not continuum and the interaction between carbon atoms and water molecules was modeled using carbon–water bond potential energy. Also, the effects of different parameters such as flow velocity, CNT's chirality, CNT's diameter, CNT's aspect ratio, elastic foundation stiffness and various end conditions on the fundamental frequencies of SWCNT's vibration were studied. Results show that by increasing the flow velocity, the natural frequencies are decreased. The molecular based water mass per unit length of CNT assumption predicts much larger natural frequencies than those predicted by continuum based one. Also, the

wall shear force calculation using continuum or molecular model results in similar fundamental frequencies.

Verification of these seemingly exotic predictions of fast transport through CNTs that emerged from the MD simulations requires fabrication of a robust test platform: a CNT membrane. Such membranes typically consist of an aligned array of CNTs encapsulated by a filler (matrix) material, with the nanotube ends opened at the top and bottom. Carbon nanotube (CNT) membranes are promising candidates for one such solution primarily because of their transport characteristics. The inner cavity of a CNT forms a natural pore with very small diameter that can in some instances be smaller than 1 nm. Moreover, smooth hydrophobic surfaces of the nanotubes lead to nearly frictionless flow of water through them, enabling transport rates that are orders of magnitude higher than transport in conventional pores. Finally, the structure of CNTs permit targeted specific modifications of the pore entrance without destroying the unique properties of the inner nanotube surface [127-131]. The combination of these three factors could enable a new generation of membranes whose transport efficiency, rejection properties, and lifetimes drastically exceed those of the current membranes.

Mostafavi et al. [132] fabricated a hollow cylindrical nanofilter with suitable mechanical strength from CNT with nanoscale porosity to remove MS_2 virus from water. Figure 20 shows that the CNTs are arranged so closely that ablock is formed and the length of the nanotube bundles is consistent to the thickness of the block. As shown in Figure 20(b), the nanofilter withsuitable porosity is prepared by closely arranging the nanotubes. Further more, Figure 20(c) shows that CNT bundle s are about 45 nm in size. The TEM image in Figure 21 shows that these entangled carbon nanotubes bundles are almost composed of MWNTs. The diameter of these carbon nanotubes among the bundles is about 30 nm. The fabricated nanofilter presents the largest pore size with a permeability of 30.7×10^{-6}m.s^{-1}Mpa^{-1} while the NF90 seems to have the smallest pore size with a low permeability of 10.5×10^{-6} m.s^{-1}Mpa^{-1}. Further, the permeability of the ESNA1-LF and NF270 are 20.3×10^{-6}m.s^{-1}Mpa^{-1} and 25.8 m.s^{-1}Mpa^{-1}, respectively. The efficiency of the virus removal by using the fabricated nanofilter was expressed by a log reduction value (LRV). Figure 22 shows filter efficiency at different pressures. With increasing pressure, the velocity of water increases through nanofilter but mass transfer velocity of virus is low and hence the different mass transfer velocity causes that the virus concentration decreases in permeate with increasing pressure. These results indicate that fabricated nanofilter can remove virus and nanoparticles from water at 20°C and pressure of about 11 bar.

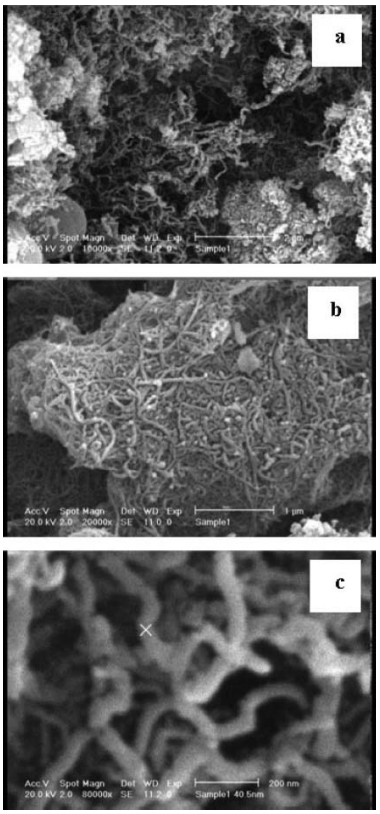

Figure 20: SEM image (a) close arranged CNT that formnanofilter, (b) porosity of naofilter, (c) carbon nanotubesbundle size [132].

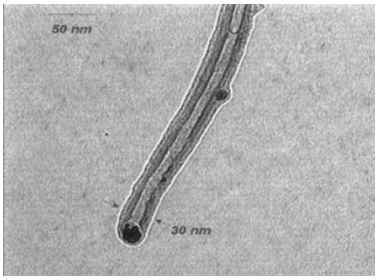

Figure 21: TEM image of MWNT with 30 nm diameter [132].

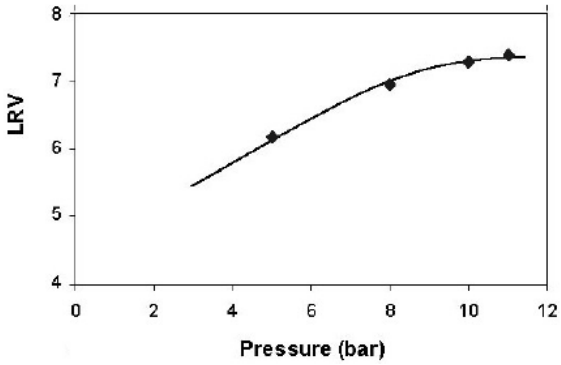

Figure 22: Filter efficiency at different pressures [132].

It should be pointed out that some different approaches to producing an aligned CNT-polymer composite membrane (Polymeric/CNT Membranes) have been investigated, such as a polypyrrole (PPy)-CNT-tyrosinase biocomposite film prepared by electrochemical polymerization [133], carbonized electrospun [134] and a MWCNT/polyaniline (PANI) multilayer film formed by alternate casting of treated MWCNT-ethanol dispersion and electrodeposition of aniline [135].

In 2006, Choi et al. [136] prepared the multi-walled carbon nanotubes (MWNTs)/polysulfone (PSf) blend membranes by a phase inversion process, using N-methyl-2-pyrrolidinone (NMP) as a solvent and water as a coagulant. Before making the blend membranes, MWNTs were first treated with strong acid to make them well dispersed in organic solvents such as NMP for the preparation of homogeneous

MWNTs/PSf blend solutions. Where: polysulfone (PSf, Udel® P 3500, Amoco, Marietta, OH) was used as a membrane material. Carbon nanotubes (multi-walled carbon nanotubes, MWNTs) manufactured by CVD process whose purity of greater than 95% were used for the modification of a PSf membrane. The MWNTs in tubular shape, composed of six-membered carbon rings, were like a rolled graphite sheet with 10–20 nm of outer diameter, 10-50μm of the length, and 4.3±2.3 nm of inner diameter. The MWNTs were surface modified with strong acids, concentrated nitric (HNO_3) and sulfuric acids (H_2SO_4) (1:3 invol. %), to make them easy to be dispersed in the organic solvents. Also, Polyvinyl pyrrolidone (PVP) with molecular weight of 55,000 g/mol and poly(ethyleneoxide) (PEO) with molecular weight of 100,000 g/mol were used for permeation tests.

Figures 23 and 24 show the FESEM photographs of the surfacesand the fractures of the MWNTs/PSf blend membranes, respectively. As one can see from Figure 23, by the MWNTs, the PSf membrane surface became rougher with increased pore size. The PSf membrane with 1.5 wt. % MWNTs looks to have the highest surface roughness and the largest pore size. These pictures suggest that the modified MWNTs with hydrophilic functional groups make the PSf membrane to have nodular structure, with increased pore size and rough surface. This result might be explained by the fast exchange of solvent and non-solvent in the phase inversion process due to the hydrophilic MWNTs.

However when the content of MWNTs increased further, especially when it was 4 wt. %, the surface structure started to become smooth again. This is maybe due to the increased viscosity of the MWNTs/PSf blend solution. As explained above, the viscosity of the blend solutions increased along with the contents of MWNTs. The increased viscosity usually retards the exchange of solvent and non-solvent, making smooth membrane surface. In such case, two factors (increased hydrophilicity and increased viscosity by the added hydrophilic MWNTs) acted at same time for the formation of the microporous blend membranes. When the content of the added MWNTs was less than 4 wt.%, increased hydrophilicity of thesolution did major role to form a nodular structure, but when it was more than 4 wt.%, increased viscosity of the solution wasthe major factor to make a smooth membrane surface.

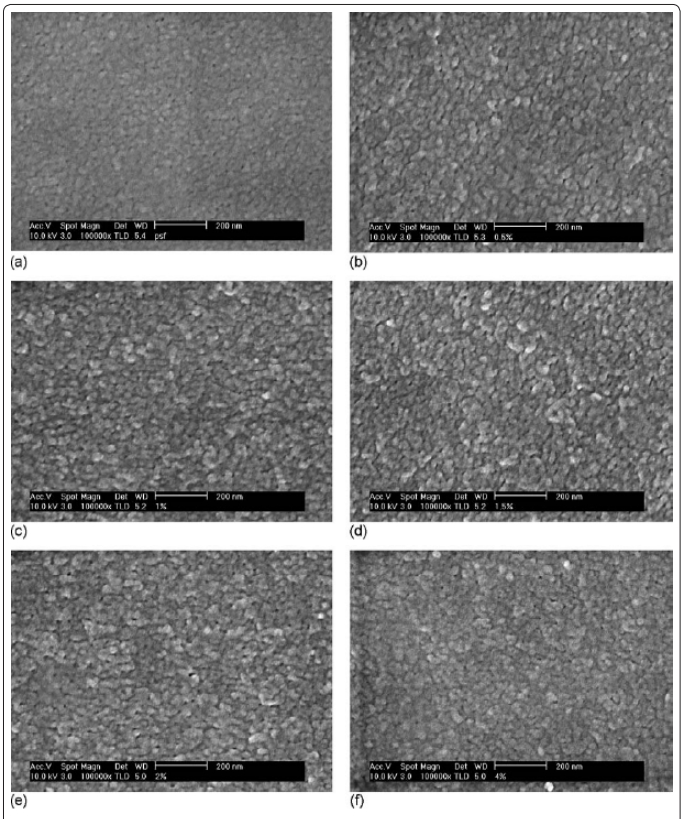

Figure 23: FESEM photographs of the surfaces of the MWNTs/PSf blend membranes with different contents of MWNTs: (a) just PSf membrane; (b) 0.5 wt.% ofMWNTs; (c) 1.0 wt.% of MWNTs; (d) 1.5 wt.% of MWNTs; (e) 2.0 wt.% of MWNTs; (f) 4.0 wt.% of MWNTs.

On the other hand, there was not a distinct difference in the structures of the fractures of the blend membranes, all showing finger like structure (Figure 24) except for the different numbers of the MWNTs positioned on the surface layer. With increasing contents of MWNTs, more MWNTs were found from the surface layer, making the membrane surface hydrophilic. Results show that the MWNTs turned out to be a good modifier for the formation of functional microporous PSf membranes, controlling the hydrophilicity of the membrane surface, adjusting the pore size and porosity. The permselective properties of the MWNTs/PSf blend membranes were appeared to be very dependent on the contents of the MWNTs used. By using proper amount of MWNTs, it was possible to increase the flux and the solute rejection at the same time for the PSf microporous membranes.

After that Peng et al. [137] described the novel nanocomposite membranes (PVA–CNT(CS)) prepared by incorporating chitosan-wrapped multiwalled carbon nanotube (MWNT)into poly(vinyl alcohol) (PVA).To fully explore the potential of CNT, two issues have to be solved. One is the serious aggregation of CNTs leading to difficulties in their manipulation and incorporation into polymeric matrixes. Another is the strong hydrophobicity leading to significant decrease of membrane selectivity. Hydrophilic modification seems a promising and feasible solution. Therefore, chitosan (CS) with distinct hydrophicility due to the existence of high proportion amino and hydroxyl groups was introducedin the study. The dispersion and solubility behavior of CNT can be remarkably improved through substantial wrappingof chitosan utilizing the emulsifying capacity of chitosan, the unique solubility behavior of chitosan. In addition, as a rigid polymer, chitosan has relatively favorable free volume characteristics. In their previous study [138], they found t hat blending chitosan into PVA matrix could considerably enhance the pervaporation performance of benzene and cyclohexane mixtures. Authors firstly investigated the free volume characteristics of PVA–CNT nanocomposite membranes by molecular dynamics simulation (using SWNT instead of MWNT in MD simulationfor simplicity) in order to theoretically elucidate whether or not CNT is an effective inorganic component to improve the pervaporation properties of PVA-based membranes according to the obtained free volume data. Four amorphous cell models forpure PVA membrane, PVA–CNT nanocomposite membrane, PVA–CS blend membrane and PVA–CNT(CS) nanocomposite membrane were constructed by molecular dynamics simulations carried out on Materials Studio (Discover and Amorphous Cell modulus) developed by Accelrys Software Inc. and shown in Figure 25. Figure 26 show the cross-section of PVA–CNT(CS)nanocomposite membrane, where the CNT content was2.0 wt.%. The CNTs wrapped by chitosan were well dispersed within PVA matrix, which indicated that chitosan was a suitable polymer to alleviate the serious aggregation of CNTs.

Results demonstrate that novel nanocomposite pervaporation

membranes composed of PVA and chitosan-wrapped CNT could exhibit simultaneous increase of permeation flux and separation factor compared with pure PVA membrane. It is supposed that the improvement originates from the appropriate physicochemical and structural characteristics of these nanocomposite membranes: (1) carbon nanotube showed preferential affinity toward benzene; (2) both carbons nanotube and chitosan could modify PVA polymer chain packing, f urther increased free volume and tailored free volumecavity size of PVA membrane.

In recent years, research on membranes with CNTs has been explored further [139-141]. However, up to now although CNTs have excellent separation, electrical and mechanical properties, and synthesis of mixed matrix membrane susing these materials have the following problems. First, during the CNTs synthesis, some impurities are produced and they must be purified by chemical or physical methods. Second, the synthesized CNTs are generally close ended and they must be cut during the purification processes or separately. Third, dispersion and dissolution of the as-grown CNTs are not usually sufficient in various organic solvents and different polymers and interaction of the interface between CNTs and polymer matrix is weak. Therefore, synthesis of highly pure, open ended and functionalized CNTs is important to form the membrane with the high quality. Nowadays, Shawky et al. [142] synthesize the multi-wall carbon nanotube (MWCNT)/aromatic polyamide (PA) nanocomposite membranes by a polymer grafting process. Polymerization was carried out in a 500 mL flask with a very high-speed magnetic stirrer. A solution of 4.326 gm (0.04 mol) of *m*-phenylene diamine and 8.48 gm (0.08 mol) of sodium carbonate in120 mL deionized water was placed in the flask. Vigorous stirring was begun and a solution of 8.12 gm (0.04 mol) of isophthaloyl chloride in150 mL of tetrahydrofuran was rapidly poured into the flask from a beaker. Stirring was continued for 5 min. The product thus obtained is a white fibrous precipitate. The polymer was separated by filtration; washed with excess deionized water and thus dried under vacuum at 80–90°C. The yield of polymer is about 100% of the theoretical value. For the preparation of MWCNT-PA composite membrane, MWCNTs were dispersed in DMAc solvent via ultrasonication for 2 h. DMAc solvent was prepared with lithium chloride salts (1% (wt./v)) as a casting solution for the PA membranes. This DMAcLiCl solution

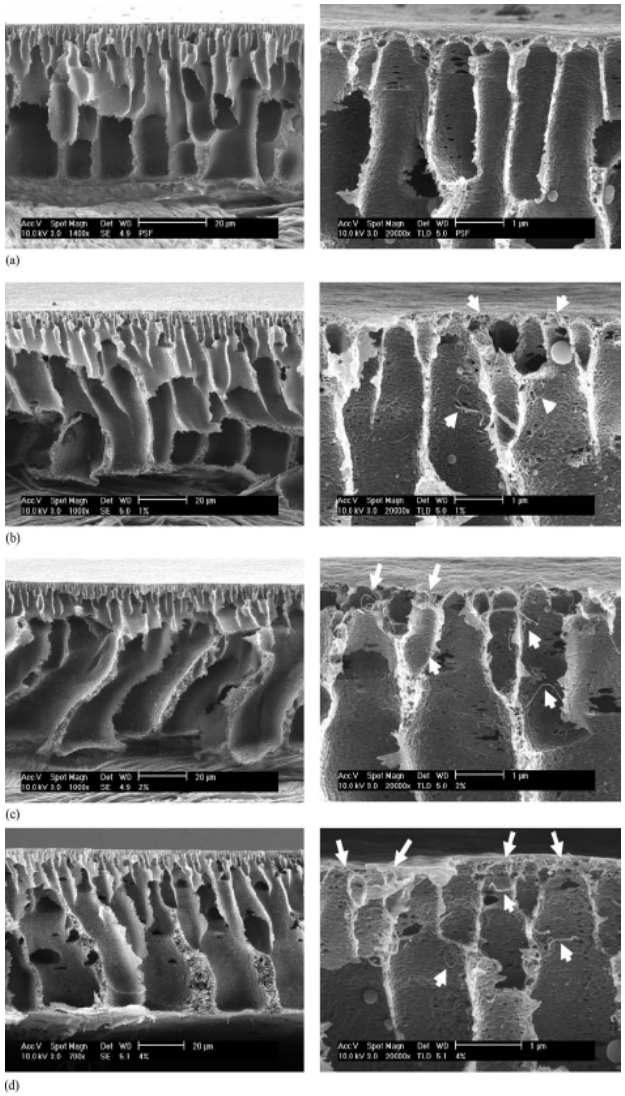

Figure 24: FESEM photographs of the cross-sections of the MWNTs/PSf blend membranes with different contents of MWNTs: (a) just PSf membrane; (b) 1.0 wt.% ofMWNTs; (c) 2.0 wt.% of MWNTs; (d) 4.0 wt.% of MWNTs.

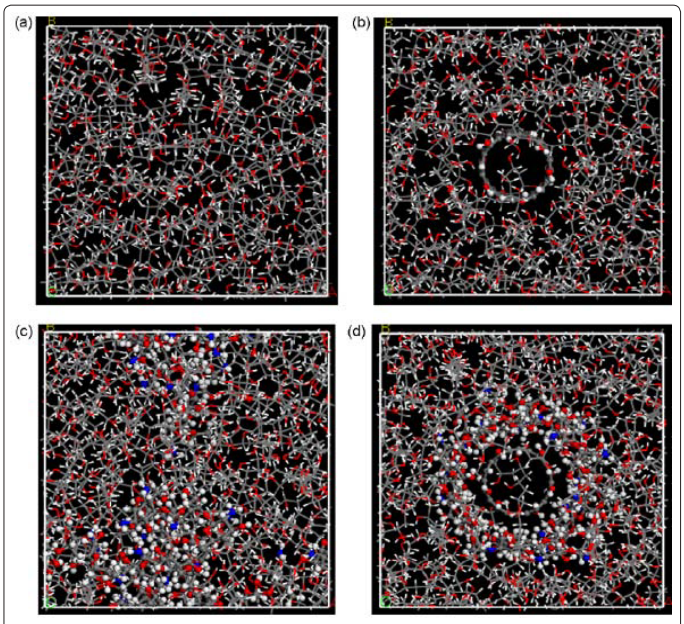

Figure 25: The amorphous cell model of pure PVA membrane (a), PVA–CNT nanocomposite membrane (b), PVA–CS blend membrane (c) and PVA–CNT(CS)nanocomposite membrane (d).

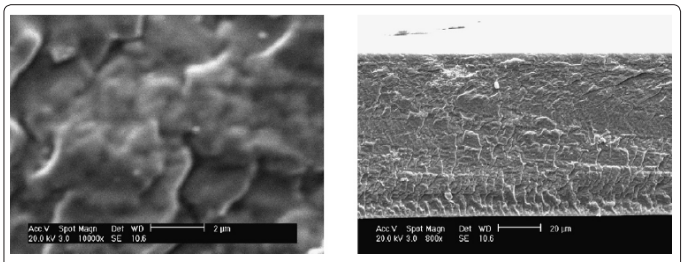

Figure 26: The SEM micrographs of the cross-section of PVA–CNT(CS) nanocomposite membrane.

was prepared by adding 0.1 g of LiClto 10 mL of DMAC and heating to complete dissolution. Multi-wall carbon nanotubes were supplied from NanoTech Labs Inc., USA, and characterized by the company as follows; purity of 95 wt.% an average diameter of 15 nm and lengths ranging from0.5 μm to 1 μm with most of the materials closer to 1 μm. The addition of benzoyl peroxide (BPO) initiator was done with the goal of forming of free-radicals on both CNTs and PA resulting in polymer-grafted nanotubes that would be better dispersed throughout the casting solution and forming morehomogenous MWCNTs-PA composite membranes. After the addition of benzoyl peroxide (BPO) initiator (0.25% (wt./v)), the mixture was heated with stirring for 3 h at 80 °C. Stirring was continued for 24 h, then the casting solution was evacuated to remove the dissolved gas, casted onto a dried clean glass Petri dish and spread with the aid of a glass rod to form a uniform thin film. A membrane thickness of 200 μm was obtained by controlling the amount of casting solution. Thus, the film was immediately placed in an oven at 90 °C for 30 min. When the solvent was completely evaporated, the Petri dish with the membrane was cooled and immersed in a deionized water bath for atleast 15 h at room temperature. Four different membranes were synthesized containing 2.5, 5, 10 and 15 mg MWCNTs/g PA,respectively with a constant PA concentration of 10% by weight inthe casting solution.

SEM imagery of the functionalized MWCNT in the resulting film showed MWCNTs to be well mixed and evenly distributed throughout the polymer matrix even at the highest concentration (Figure 27) in contrast with earlier efforts to create CNT/polymer composite membranes where CNTs were non-uniformly distributed. No evidence was observed of CNT clustering, even as CNT concentration increased to 15 mg MWCNT/g PA. Results show that the addition of MWCNTs to the PA membranes to form a nanocomposite structure improved the mechanical properties of these membranes and their ability to reject key contaminants with little compromise in membrane permeability. However, there may be a reduction in longer-term membrane performance due to adsorptive fouling since the addition of MWCNTs increased membrane hydrophobicity. Additional factors to consider in the development of thesecomposites include the need to balance the dimensions of the membrane film cast with those of the reinforcing

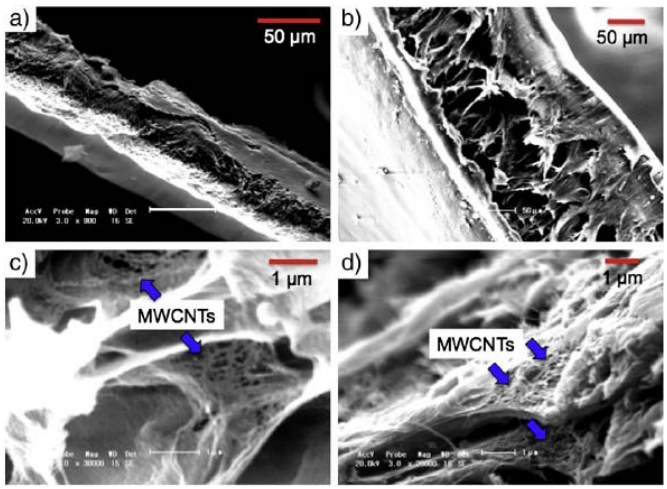

Figure 27: Representative cross-sectional SEM images of a) a control membrane without MWCNTs, b) a nanocomposite membrane with 2.5 CNTs (mg/g), c) a nanocomposite membranewith 5 CNTs (mg/g), and d) a nanocomposite membrane with 15 CNTs (mg/g).

CNTs, and the effectof derivative CNTs on membrane casting and performance.

In order to investigate the protein fouling behavior of carbon nanotube/polyethersulfone composite membranes during water filtration, Celik et al. [143,144] prepared the multi-walled carbon nanotube/polyethersulfone (C/P) composite membranes via the phase inversionmethodwith bovine serum albumin (BSA) and ovalbumin (OVA) used as the model protein for assessing the protein fouling behavior.

To prepare the composite membranes, functionalized MWCNTs were dispersed homogenously in NMP prior to dissolving 20% PES in the blend solution while continuously stirring and heating at 60°C until the solution became completely homogenous. The resultant polymer solution was ultrasonicated to allow a complete release of air bubbles. The blend solution was then casted on a glass plate using a casting knife at room temperature, and the glass plate was immersed in a coagulation bath of DI water. The pristine membranes were peeled off and subsequently rinsed with and stored in DI water until use. Note that membranes marked as C/P-0% refer to the original polyethersulfone membrane and C/P-4% refers to the membranes prepared in a casting solution in which the amount of MWNTswith respect to polyethersulfone was 4% by weight.

The adsorption of BSA onto C/P composite membranes is demonstrated in Figure 28. At pH 3, electrostatic attraction ccurred since the protein and all composite membranes had opposite charges. Moreover, at pH values below the IEP, the protein denaturation is relatively high. Hence, at pH 3 a higher amount of protein adsorption was observed on the membranes. At pH 7, both BSA and composite membrane surfaces were negatively charged, and electrostatic repulsion was dominant between the membrane surfaces and the protein. In this case, protein adsorption decreased with an increasing amount of MWCNTs in the blend solution, at both pH 3 and pH 7, due to the increased hydrophilicity of the composite membranes. And even though the protein adsorption decreased with increasing amounts of MWCNTs in the membrane structure, the protein adsorptions on the C/P-2% and C/P-4% membranes were similar at a 95% confidence level, probably due to the similar hydrophilicity of these two membranes.

Results show that the C/P composite membranes were fouled less compared to the barepolyethersulfone (PES) membrane at 4 h of static protein adsorption at neutral pH. Moreover, the irreversible fouling ratio of the C/P composite membranes was less than the bare PES membrane after 1 h of protein ultrafiltration, and the flux recovery ratio of the C/P composite membranes was higher than the bare PES membrane after 20 min of DI water filtration. Based on these results, C/P composite membranes were shown to have the potential to alleviate the effects of protein fouling, thereby enabling C/P composite membranes to be used for several runs of protein filtration after simple washing with water.

It should be realized that the most promising property of CNT membranes for water purification applications is their extremely high permeability [145,146]. This property should translate into more water per unit of applied pressure, more efficient, smaller purification units and ultimately into lower purification or desalinations costs. Rich possibilities for chemical functionalization, coupled with the rather unique ability to manipulate only the chemistry at the nanotube mouth open up the possibility of producing membranes tailored for specific

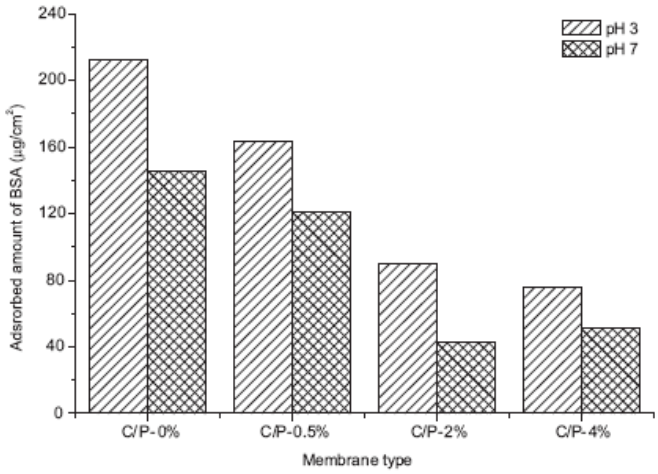

Figure 28: BSA adsorption on the C/P composite membranesat pH 3 and pH 7 (average BSA adsorption of two replicatesare reported).

applications (e.g., RO desalination or impurity purification) while maintaining the basic membrane structure and high permeability.

However, a true assessment of the potential impact of CNT membranes on water purification (and specifically on water desalination) applications requires a more comprehensive comparison of the membrane characteristics with the general requirements of the membrane purification process. At least in the case of RO desalination, the process efficiency comes from three main sources: capital costs, energy costs, and operation costs (which include costs for pretreatment, post treatment, and membrane cleaning and regeneration).

Meanwhile, the CNT technology is still in its infancy; therefore, most attempts at quantitative evaluation will face large uncertainties associated with predicting the future technological milestones, or the fact that some of the major membrane characteristics (e.g., fouling properties) have not been sufficiently evaluated. Another large source of uncertainty is the lack of availability and cost estimates for a manufacturing process that allows scale-up of membrane fabrication. However, some qualitative conclusions based even on the limited set of data that is available now can be still reached. The high flux of CNT membranes provides a clear advantage for both the energy costs and the capital costs, as the same amount of product water could be obtained with smaller driving pressures and less membrane area. But, some of the other important advantages of CNT membrane technology could come from the factors contributing to the third cost factor: the operation costs. The uniform pore size of CNT membranes could simplify or even eliminate the requirements for complicated multistage pretreatment efforts. The membrane pore surface is also rather chemically inert, which could increase the membrane lifetime against the harsh agents used for pretreating water before RO or other purification steps. Unlike most polymeric membrane surfaces, the CNT membrane surface is hydrophilic; therefore, it could offer an increased resistance to fouling, as well as easier cleanup by rinsing or backwashing. These factors could all contribute to an increased membrane lifespan and ultimately to operation cost savings.

If considering these factors, it becomes clear that the real impact of CNT membrane technology may lie in its potential to improve all of the major areas that contribute to the costs of water purification processes. Clearly, much work needs to be done before these promises translate into field applications. Researchers need to develop approaches for fabricating CNTs with an even narrower distribution of the pore sizes, ideally with pores that are less than1 nm. Targeted chemical modification of the pore entrances should improve dramatically the rejection characteristics of the membrane. Further studies are necessary to quantify the membrane fouling resistance and useful lifespan. Finally, development of large-scale, low-cost manufacturing processes is imperative to ensure that CNT membrane technology can achieve significant penetration into the water purification market.

Issueson human health and environmental effects

To date, nanotechnology continues to evolve and develop at breakneck speed. Many nano-based applications are already available commercially but little is known about the human health and environmental effects of exposure. This rapid surge in worldwide research and development and the potential large-scale use of nanomaterials in consumer products point toward the need for more definitive information regarding environmental health and safety impacts from the manufacturing process, disposal (industrial or personal), remediation, and treatment applications. It is noted that the applications now show enormous promise for improving public health and the environment—specifically water quality. However, because of nanomaterials' exceedingly small size, the assumption is that they will be extremely mobile in porous media, thereby increasing the likelihood of human exposure due to dispersion and potential persistence in the environment. Yet, how reactive such materials could be in the environment, what residual compounds are formed during degradation, and where and how these materials partition to various environmental and biological media are crucial but largely unknown. How these materials move from one medium to another, from one organism or ecosystem to another, and from organisms to the environment and vice versa will be critical for understanding and implementing proper manufacturing, usage, and recycling/disposal options that are most protective of human health and the environment. In order to effectively assess these impacts, a full life-cycle perspective (impact of a product from the accumulation of starting materials to the development, manufacture, use, and eventual disposal or reuse of the item or portions thereof) of the various constituents and end products is an important component of a research framework. Although complete, robust life-cycle analyses are difficult, and potentially impossible, when data is limited, and this should not be an excuse for ignoring the full life cycle in any risk analysis.

Current&future developments

For the application in a desalination process, the distinguished membranes must exhibit a number of characteristics such as high water flux, high salt rejection, mechanical stability, resistance to fouling, and low cost. A number of polymer materials such as cellulose acetates, thin film composite (TFC) polyamides, cross-linked poly(furfuryl alcohol) and sulfonated polyethersulfone have been investigated for desalination. Although cellulose acetates and TFC polyamides have been the most successful, cellulose acetate membranes slowly hydrolyze overtime, are easily attacked by bacteria, and generally are not used above 35°C. Aromatic polyamides, although without those problems, have low resistance to fouling, as well as a low chlorine tolerance due to the existence of secondary amides and electron-rich aromatic rings. The currently available substrates used for the preparation of TFC membranes include polysulfone and polyethersulfone. Most of these membrane substrates, however, have relatively poor chemical

and thermal stabilities, and for ultrafiltration (UF) are susceptible to performance degradation caused by fouling. Therefore, the development of more thermally and chemically resistant selective top layers and substrates is critically required for water purification.

Up to now, mostpressure-driven membranes are in these two categories, that is, phase separation membranes and thin film composite (TFC) membranes. According to pore diameters, there are four categories of pressure-driven membranes—these include microfiltration (MF), ultrafiltration (UF), nanofiltration (NF) and reverse osmosis (RO) membranes. Nanofiltration, defined by many "as a process between Ultrafiltration (UF) and Reverse Osmosis (RO)," is a relatively recent technology, largely developed over the past decade. Typically, NF membranes have sodium chloride rejections between 20 and 80 percent and molecular weight cutoffs for dissolved organic solutes of 200-1000 Dalton. Their low-pressure operation (4-14 bars) provides increased energy savings with significantly lower installation and operating costs. A number of polymer materials have been investigated for NF applications. For instance:

Cellulose acetate (CA) membrane and polyamide TFC membrane have been the most successful:

1. Cellulose acetate membranes. Cellulose is a linear, rod-like material that renders membranes mechanically robust. Cellulose acetate was the first high-performance NF/RO membrane material discovered. Today, CA membranes still maintain a small fraction of the market because they are easy to make, mechanically tough and resistant to degradation by chlorine up to 1 ppm. However, CA membranes slowly hydrolyze over time and are stable only in the pH range of 4-6. Salt rejection decreases as temperature increases and therefore CA membranes are generally not used above 35°C. In addition, they are easily attacked by bacteria.

2. Polyamide TFC membranes. A more successful, commercially available NF/RO membrane is the TFC aromatic polyamide membrane. This type of membrane has higher salt rejections and fluxes than CA membranes. On the other hand, aromatic polyamides have several disadvantages including:

a. Low resistance to fouling. Membrane fouling (scale, silt, biofouling, organic fouling, *etc.*) is the main cause of permeate flux decline and loss of water quality. Fouling can decrease total throughput more than 30 percent, and further increase capital costs by 15 percent resulting from membrane cleaning.

b. Limited oxidant tolerance due to the existence of secondaryamides and electron-rich aromatic rings. Selectivity is rapidlyand permanently lost once exposed to feed water containingmore than a few ppb levels of chlorine or hypochloritedisinfectants. It creates major problems in designing foreffective pretreatment of chlorine to destroy microorganisms.

c. Chemical and thermal instabilities. The substrate layer of TFC membranes, usually polysulfone, is attacked by many solvents,which limits deposition of a permselective, ultrathin membranefrom solvent systems, such as Dimethylformamide (DMF),and N-methyl-pyrrolidone (NMP). Most TFC membranescan only be used below 30-50°C because of limitations of the polysulfone. On the other hand, hot wastewater from the food, chemical, and petroleum processing industries are discharged directly and the energy lost is estimated at higher percent of the total energy consumption. Developing chemically stable substrates, which operate at higher temperatures, will result in substantial energy savings. Therefore, the development of more thermally and chemically resistant selective top layers and substrates is critically required for water purification.

With new breakthroughs in membrane technology, constituent specific membranes are a possibility. Research in the use of embedded "nanoparticles" in reverse osmosis membranes has shown promise and may be applicable to nanofiltration membranes in the future. Meanwhile, the issues of nanomaterials leaching out from the membranes with its relevant contamination should be investigated in detail.

Conflict of interest

The author declares no conflict of interest.

Acknowledgement

This work is supported by City University of Hong Kong Strategic Research Grant (SRG) No.7002582.

References

1. Rejeski D, Michelson ES (2009) International governance perspectives on nanotechnology water innovation. Nanotech Appl Clean Water 509-519.
2. Brame J, Li QL, Alvarez PJJ (2011) Nanotechnology-enabled water treatment and reuse: emerging opportunities and challenges for developing countries. Trends in Food Sci& Tech 22: 618-624.
3. Street A, Duncan JS, Savage N (2009) Nanotechnology in water: societal, ethical, and environmental considerations. Nanotech Appl Clean Water 453-462.
4. Gorman ME, Wardak A, Fauss E, Swami N (2009) A Framework for using nanotechnology to improve water quality. Nanotech Appl Clean Water 491-507.
5. Diallo MS, Duncan JS, Savage N, Street A, Sustich R (2009) Nanotechnology solutions for improving water quality. Nanotech Appl Clean Water 585-587.
6. Greaves I, Hunt P (2010) Terrorism in Perspective. Responding to Terrorism 1-43.
7. Gray NF (2010) Sustainability principles in water management. Water Tech 711-26.
8. Somlyódy L (1995) Water quality management: Can we improve integration to face future problems? Water Sci Tech 31: 249-259.
9. Arnell NW (2004) Climate change and global water resources: SRES emissions and socio-economic scenarios. Global Environ Change 14: 31-52.
10. Ghosh S, Mujumdar PP (2006) Risk minimization in water quality control problems of a river system. Advances Water Resour 29: 458-470.
11. Jury WA, Vaux Jr HJ (2007) The emerging global water crisis: Managing scarcity and conflict between water users. Advances in Agronomy 95: 1-76.
12. Hoff H (2009) Global water resources and their management. Current Opinion Environ Sustain 1: 141-147.
13. Rubio-Castro E, Ponce-Ortega JM, Serna-González M, Jiménez-Gutiérrez A, El-Halwagi MM (2011) A global optimal formulation for the water integration in eco-industrial parks considering multiple pollutants. Computer ChemEng 35: 1558-1574.
14. Ashby MF, Ferreira PJ, Schodek DL (2009) Nanomaterials and nanotechnologies: An overview. Nanomaterials: Nanotechnologies and Design 1-16.
15. Kostoff RN, Koytcheff RG, Lau GY (2007) Global nanotechnology research literature overview. Technological Forecasting and Social Change 74: 1733-1747.
16. Pitkethly MJ (2004) Nanomaterials-the driving force. Mater Today 7: 20-29.
17. Ashby MF, Ferreira PJ, Schodek DL (2009) Nanomaterials synthesis and characterization. Nanomaterials: Nanotechnologies and Design 257-290.

18. Ashby MF, Ferreira PJ, Schodek DL (2009) Nanomaterials and nanotechnologies in health and the environment. Nanomaterials: Nanotechnologies and Design 467-500.

19. Van Hove MA (2009) Atomic-scale structure: From surface to nanomaterials. Surf Sci 603: 1301-1305.

20. Zäch M, Hägglund C, Chakarov D, Kasemo B (2006) Nanoscience and nanotechnology for advanced energy systems. CurrOpin Solid State Mater Sci 10: 132-43.

21. Hühnerfuss H, Shah MR (2009) Enantioselective chromatography—A powerful tool for the discrimination of biotic and abiotic transformation processes of chiral environmental pollutants. J Chromato A 1216: 481-502.

22. Koopmans RJ, Aggeli A (2010) Nanobiotechnology — quo vadis? Current Opin Microbiol 13: 327-334.

23. Wong IY, Almquist BD, Melosh NA (2010) Dynamic actuation using nano-bio interfaces. Mater Today 13: 14-22.

24. Huh AJ, Kwon YJ (2011) "Nanoantibiotics". A new paradigm for treating infectious diseases using nanomaterials in the antibiotics resistant era. J Control Release 156: 128-145.

25. Yan XH, Liu GJ, Dickey M, Willson CG (2004) Preparation of porous polymer membranes using nano- or micro-pillar arrays as templates. Polymer 45: 8469-8474.

26. Yan L, Li YS, Xiang CB, Shun XD (2006) Effect of nano-sized Al2O3-particle addition on PVDF ultrafiltration membrane performance. J Membrane Sci 276: 162-167.

27. Vaughan BR, Marand E (2008) Transport properties of polymer–aluminophosphatenano-composites prepared by simple mixing. J Membrane Sci 310: 197-207.

28. Rahimpour A, Madaeni SS, Mansourpanah Y (2010) Nano-porous polyethersulfone (PES) membranes modified by acrylic acid (AA) and 2-hydroxyethylmethacrylate (HEMA) as additives in the gelation media. J Membrane Sci 364: 380-388.

29. Rahimpour A, Jahanshahi M, Rajaeian B, Rahimnejad M (2011) TiO_2 entrapped nano-composite PVDF/SPES membranes: Preparation, characterization, antifouling and antibacterial properties. Desalination.

30. Liu F, Moghareh Abed MR, Li K (2011) Preparation and characterization of poly (vinylidene fluoride) (PVDF) based ultrafiltration membranes using nano γ-Al_2O_3. J Membrane Sci 366: 97-103.

31. Reijnders L (2006) Cleaner nanotechnology and hazard reduction of manufactured nanoparticles. J Cleaner Produc 14: 124-133.

32. Anshup TP (2009) Noble metal nanoparticles for water purification: A critical review. Thin Solid Films 517: 6441-6478.

33. Diallo MS, Duncan JS, Savage N, Street A, Sustich R (2009) Nanotechnology-Based Membranes for Water Purification. Nanotech Appl Clean Water 47-58.

34. Kim KD, Han DN, Lee JB (2006) Formation and characterization of Ag-deposited TiO2 nanoparticles by chemical reduction method. Scrip Mater 54: 143-146.

35. Keleher J, Bashant B, Heldt N, Johnson L, Li Y (2002) Photo-catalytic preparation of silver-coated TiO_2 particles for antibacterial applications. World J Microbio Biotech 18: 133-139.

36. Kim J, Cho M, Oh B, Choi S, Yoon J (2004) Control of bacterial growth in water using synthesized inorganic disinfectant. Chemosphere 55: 775-780.

37. Butkus MA, Edling L, Labare MP (2003) The efficacy of silver as a bactericidal agent: advantages, limitations and considerations for future use. J Water Supply: Res Tech-AQUA 52: 407-416.

38. Remy H (1956) Treatise on Inorganic Chemistry. New York, s.n.

39. Yoshihiro I (2002) Bactericidal activity of Ag zeolite mediated by reactive species under aeratedconditions. J Inorganic Biochem 92: 37-42.

40. Kumar VS, Nagaraja BM, Shashikala V, Padmasri AH, Madhavendra SS te al. (2004) Highly efficient Ag/C catalyst prepared by electrodeposition method in controlling microorganisms in water. J Molecular Catalysis A: Chemical 223: 313-319.

41. Logenberger L, Mills G (1995) Formation of metallic particles in aqueous solutions by reactions of metal complexes with polymers. J Phys Chem 99: 475-478.

42. Wang YL, Wan YZ, Dong XH, Cheng GX, Tao HM et al. (1998) Preparation and characterization of antibacterial viscose-based activated carbon fiber supporting silver. Carbon 36: 1567-1571.

43. Pape HL, Solano-Serena F, Contini P, Devillers C, Maftah A, et al. (2002) Evaluation of the anti-microbial properties of an activated carbon fibre supporting silver using a dynamic method. Carbon 40: 2947-2954.

44. Murugan K, Rao TN, NarashimaRao GV, Gandhi AS, Murty BS (2011) Effect of dehydration rate on non-hydrolytic TiO_2 thin film processing: Structure, optical and photocatalytic performance studies. Mater ChemPhy 129: 810-815.

45. Pomorska A, Yliniemi K, Wilson BP, Shchukin D, Johannsmann D, et al. (2011) QCM study of the adsorption of polyelectrolyte covered mesoporous TiO_2nanocontainers on SAM modified Au surfaces. J Colloid Interface Sci 362: 180-187.

46. Babu VJ, Nair AS, Zhu PN, Ramakrishna S (2011) Synthesis and characterization of rice grains like Nitrogen-doped TiO_2 nanostructures by electrospinning–photocatalysis. Mater Lett 65: 3064-3068.

47. Li Q, Liang W, Shang JK (2007) Enhanced visible-light absorption from pdo nanoparticles in nitrogen-doped titanium oxide thin films. Appl Phys Lett 90.063109.

48. Li Q, LY W, Wu P, Xie R, Shang JK (2008) Palladium oxide nanoparticles on nitrogen doped titanium oxide: accelerated photocatalytic disinfection and post-illumination catalytic "Memory". Adv Mater 20: 3717-3723.

49. Li Q, Li YW, Liu ZQ, Xie RC, Shang JK (2010) Memory antibacterial effect fromphotoelectron transfer between nanoparticles and visible light photocatalyst. J Mater Chem 20: 1068-1072.

50. Wu PG, Imlay JA, Shang JK (2010) Mechanism of *Escherichia coli* inactivation on palladium-modified nitrogen-doped titanium dioxide.Biomater 31: 7526-7533.

51. Asahi R, Morikawa T, Ohwaki T, Aoki K, Taga Y (2001) Visible-light photocatalysis in nitrogen-doped titanium oxides. Science 293: 269-271.

52. Sakthivel S,Kisch H (2003) Photocatalytic and photoelectrochemical properties of nitrogen doped titanium dioxide. Chem Phys Chem 4: 487-490.

53. Burda C, Lou Y, Chen X, Samia ACS, Stout J et al. (2003) Enhanced nitrogen doping in TiO_2 nanoparticles. Nano Letters 3: 1049-1051.

54. Li Q, Xie R, Mintz EA, Shang JK (2007) Effect of precursor ratio on synthesis and optical absorption of TiON photocatalytic nanoparticles. J Amer Ceramic Soci 90: 1045-1050.

55. Jiang Y, Zhang P, Liu ZW, Xu F (2006) The preparation of porous nano-TiO_2 with high activity and the discussion of the cooperation photocatalysis mechanism. Mater ChemPhy 99: 498-504.

56. Liu BS, Wen LP, Zhao XJ (2008) The study of photocatalysis under ultraviolet + visible two-beam light irradiation using undoped nano-titanium dioxide. Mater Chem Phy 112: 35-40.

57. Cui LF, Huang F, Niu MT, Zeng LW, Xu J et al. (2010) A visible light active photocatalyst: Nano-composite with Fe-doped anatase TiO_2 nanoparticles coupling with TiO_2(B) nanobelts. J Molecular Cataly A: Chem 326: 1-7.

58. Liu BS, Zhao XJ (2010) A kinetic model for evaluating the dependence of the quantum yield of nano-TiO_2 based photocatalysis on light intensity, grain size, carrier lifetime, and minority carrier diffusion coefficient: Indirect interfacial charge transfer. Electrochimica Acta 55: 4062-4070.

59. Sarasidis VC, Patsios SI, Karabelas AJ (2011) A hybrid photocatalysis–ultrafiltration continuous process: The case of polysaccharide degradation. Separation Purification Tech 80: 73-80.

60. Chen EZ, Su HJ, Zhang WY, Tan TW (2011) A novel shape-controlled synthesis of dispersed silver nanoparticles by combined bioaffinity adsorption and TiO_2photocatalysis. Powder Tech 212: 166-172.

61. Choi H, Al-Abed SR, Dionysiou DD, Stathatos E, Lianos P (2010) TiO_2-based advanced oxidation nanotechnologies for water purification and reuse. Sustainability Sci and Eng 2: 229-254.

62. Rosen MJ (2004) Surfactants and Interfacial Phenomena.3rd edition, Hoboken, NJ, Wiley-Interscience.

63. Stathatos E, Choi H, Dionysiou DD (2007) A simple procedure of making room temperaturemesoporous TiO_2 films with high purity and enhanced photocatalytic activity. Environ Eng Sci 24: 13-20.

64. Ollis DF, Al-EkabiH (Eds.) (1993) Photocatalytic purification and treatment of water and air. Elsevier Science, Amsterdam, The Netherlands.

65. Bruni L, Bandini S (2008) The role of the electrolyte on the mechanism of charge formation in polyamide nanofiltration membranes. J Membrane Sci 308: 136-151.

66. Madaeni SS, Zinadini S, Vatanpour V (2011) A new approach to improve antifouling property of PVDF membrane using in situ polymerization of PAA functionalized TiO2 nanoparticles. J Membrane Sci.

67. Rahimpour A, Madaeni SS, Ghorbani S, Shockravi A, Mansourpanah Y (2010) The influence of sulfonated polyethersulfone (SPES) on surface nano-morphology and performance of polyethersulfone (PES) membrane. Applied Surf Sci 256: 1825-1831.

68. Rahimpour A, Jahanshahi M, Rajaeian B, Rahimnejad M (2011) TiO2 entrapped nano-composite PVDF/SPES membranes: Preparation, characterization, antifouling and antibacterial properties. Desalination.

69. Han RL, Zhang SH, Liu C, Wang YT, Jian XG (2009) Effect of NaA zeolite particle addition on poly(phthalazinone ether sulfone ketone) composite ultrafiltration (UF) membrane performance. J Membrane Sci 345: 5-12.

70. Dong FL, Li ZF, Wang SW, Xu LJ, Yu XJ (2011) Preparation and properties of sulfonatedpoly(phthalazinone ether sulfone ketone)/zirconium sulfophenylphosphate/PTFE composite membranes. Inter J Hydro Ener 36: 3681-3687.

71. Yang YN, Zhang HX, Wang P, Zheng QZ, Li J (2007) The influence of nano-sized TiO2 fillers on the morphologies and properties of PSF UF membrane. J Membrane Sci 288: 231-238.

72. Zhang YQ, Shan X, Jin ZH, Wang YL (2011) Synthesis of sulfated Y-doped zirconia particles and effect on properties of polysulfone membranes for treatment of waste water containing oil. J Hazardous Mater 192: 559-567.

73. Parshetti GK, Doong RA (2009) Dechlorination of trichloroethylene by Ni/Fe nanoparticles immobilized in PEG/PVDF and PEG/nylon 66 membranes. Water Res 43: 3086-3094.

74. Meng ZH, Liu HL, Liu Y, Zhang J, Yu SL et al. (2011) Preparation and characterization of Pd/Fe bimetallic nanoparticles immobilized in PVDF·Al_2O_3 membrane for dechlorination of monochloroacetic acid. J Membrane Sci 372: 165-171.

75. Fang ZQ, Qiu XH, Chen JH, Qiu XQ (2011) Debromination of polybrominated diphenyl ethers by Ni/Fe bimetallic nanoparticles: Influencing factors, kinetics, and mechanism. J Hazardous Mater 958-969.

76. Parshetti GK, Doong RA (2011) Synergistic effect of nickel ions on the coupled dechlorination of trichloroethylene and 2, 4-dichlorophenol by Fe/TiO_2nanocomposites in the presence of UV light under anoxic conditions. Water Res 45: 4198-4210.

77. Wu LF, Ritchie MC (2006) Removal of trichloroethylene from water by cellulose acetate supported bimetallic Ni/Fe nanoparticles. Chemosphere 63: 285-292.

78. Diao MH, Yao MS (2009) Use of zero-valent iron nanoparticles in inactivating microbes. Water Res 43: 5243-5251.

79. Tyrovola K, Peroulaki E, Nikolaidis NP (2007) Modeling of arsenic immobilization by zero valent iron. Euro J Soil Bio 43: 356-367.

80. Barnes RJ, van der Gast CJ, Riba O, Lehtovirta LE, Prosser JI et al. (2010) The impact of zero-valent iron nanoparticles on a river water bacterial community. J Hazardous Mater 184: 73-80.

81. Ouyang L, Malaisamy R, Bruening ML (2008) Multilayer polyelectrolyte films as nanofiltration membranes for separating monovalent and divalent cations. J Membrane Sci 310: 76-84.

82. Malaisamy R, Talla-Nwafo A, Jones KL (2011) Polyelectrolyte modification of nanofiltration membrane for selective removal of monovalent anions. Separation Purification Tech 77: 367-374.

83. Ji YL, An QF, Zhao Q, Chen HL, Qian JW et al. (2010) Fabrication and performance of a new type of charged nanofiltration membrane based on polyelectrolyte complex. J Membrane Sci 357: 80-89.

84. Hu LH, Flanders PM, Miller PL, Strathmann TJ (2007) Oxidation of sulfamethoxazole and related antimicrobial agents by TiO2 photocatalysis. Water Res 41: 2612-2626.

85. Lin YC, Lee HS (2010) Effects of TiO2 coating dosage and operational parameters on a TiO_2/Ag photocatalysis system for decolorizing Procion red MX-5B. J Hazardous Mater 179: 462-470.

86. Ma N, Zhang YB, Quan X, Fan XF, Zhao HM (2010) Performing a microfiltration integrated with photocatalysis using an Ag-TiO_2/HAP/Al_2O_3 composite membrane for water treatment: Evaluating effectiveness for humic acid removal and anti-fouling properties. Water Res 44: 6104-6114.

87. Pastoriza-Santos I, Liz-Marzan LM (1999) Formation and stabilization of silver nanoparticles through reduction by N, N-Dimethylformamide. Langmuir 15: 948-951.

88. Mulder M (1996) Basic Principles of Membrane Technology.2nd edition, Dordrecht, The Netherlands, Kluwer Academic Publishers.

89. Savage N, Diallo M (2005) Nanomaterials and water purification: opportunities and challenges. J Nanoparticle Res 7: 331-342.

90. Renn O, Roco MC (2006) Nanotechnology and the need for risk governance. JNanoparticle Res 8: 153-191.

91. Komarneni S (1992) Nanocomposites. J Mater Chem 2: 1219-1230.

92. Moore TT, Mahajan R, Vu DQ, Koros WJ (2004) Hybrid membrane materials comprising organic polymers with rigid dispersed phases. AIChE Journal 50: 311-321.

93. Jeong BH, Hoek EMV, Yan YS, Subramani A, Huang XF, et al. (2007) Interfacial polymerization of thin film nanocomposites: a new concept for reverse osmosis membranes. J Membrane Sci 294: 1-7.

94. Mary Theresa M Pendergast, Jodie M Nygaard, Asim K. Ghosh, Eric MV Hoek (2010) Using nanocomposite materials technology to understand and control reverse osmosis membrane compaction. Desalination 261: 255-263.

95. Mahdi Fathizadeh, Abdolreza Aroujalian, Ahmadreza Raisi (2011) Effect of added NaXnano-zeolite into polyamide as a top thin layer of membraneon water flux and salt rejection in a reverse osmosis process. J Membrane Sci 375: 88-95.

96. Giorno L, Mazzei R, Drioli E (2010) Biological membranes and biomimetic artificial membranes. Comprehensive Membrane Sci Eng 1: 1-12.

97. Hutchens SA, Benson RS, Evans BR, O'Neill HM, Rawn CJ (2006) Biomimetic synthesis of calcium-deficient hydroxyapatite in a natural hydrogel. Biomater 27: 4661-4670.

98. Novak MT, Bryers JD, Reichert WM (2009) Biomimetic strategies based on viruses and bacteria for the development of immune evasive biomaterials. Biomater 30: 1989-2005.

99. Guo ZG, Liu WM, Su BL (2011) Super hydrophobic surfaces: From natural to biomimetic to functional. J Colloid Interface Sci 353: 335-355.

100. Liu HJ, Qu JH, Dai RH, Ru J, Wang ZJ (2007) A biomimetic absorbent for removal of trace level persistent organic pollutants from water. Environ Pollution 147: 337-342.

101. James D, Gladis JM, Pandey AK, Naidu GRK, Rao TP (2008) Design of two-dimensional biomimetic uranyloptrode and its application to the analysis of natural waters. Talanta 74: 1420-1427.

102. Lee KP, Arnot TC, Mattia D (2011) A review of reverse osmosis membrane materials for desalination—Developmentto date and future potential. J Membrane Sci 307: 1-22.

103. Lee KP, Arnot TC, Mattia D (2011) A review of reverse osmosis membrane materials for desalination—Development to date and future potential. J Membrane Sci 370: 1-22.

104. Avlonitis SA, Kouroumbas K, Vlachakis N (2003) Energy consumption and membrane replacement cost for seawater RO desalination plants. Desalination 157: 151-158.

105. SpieglerKS, El-Sayed YM (1994) A Desalination Primer: Introductory Book for Students and Newcomers to Desalination. Balaban Desalination Publications.

106. Shannon M, Bohn P, Elimelech M, Georgiadis J, Marinas B et al. (2008) Science and technology for water purification in the coming decades. Nature 452: 301-310.

107. Iijima S (1993) Single-shell carbon nanotubes of 1-nm diameter. Nature 363: 603-605.

108. Iijima S (1991) Helical microtubules of graphitic carbon. Nature 354: 56-58.

109. Dupuis AC (2005) The catalyst in the CCVD of carbon nanotubes—a review. Progress Mater Sci 50: 929-961.

110. Terrones M (2003) Science and technology of the twenty-first century: synthesis, properties and applications of carbon nanotubes. Annual Rev Mater Res 33: 419-501.

111. Meille V (2006) Review on methods to deposit catalysts on structured surfaces. Appl Catalysis A: Gerneral 315: 1-17.

112. García-Céspedes J, Rubio-Roy M, Polo MC, Pascual E, Andújar JL, et al. (2007) Carbon nanotubes grown by asymmetric bipolar pulsed-DC PECVD. Diamond Related Meter 16: 1131-1135.

113. Zhuo CW, Hall B, Richter H, Levendis Y (2010) Synthesis of carbon nanotubes by sequential pyrolysis and combustion of polyethylene. Carbon 48: 4024-4034.

114. Yamada T, Namai T, Hata K, Futaba DN, Mizuno K, et al. (2006) Size-selective growth of double-walled carbon nanotube forests from engineered iron catalysts. NatureNanotech 1: 131-136.

115. Bouchet-Fabre B, Fadjié-Djomkam A, Fernandez-Pacheco R, Delmas M, Pinault M, et al. (2011) Effect of tantalum nitride supporting layer on growth and morphology of carbon nanotubes by thermal chemical vapor deposition. Diamond Related Mater 20: 999-1004.

116. Seah CM, Chai SP, Mohamed AR (2011) Synthesis of aligned carbon nanotubes. Carbon.

117. Futaba DN, Hata K, Yamada T, Hiraoka T, Hayamizu Y, et al. (2006) Shape engineerable and highly densely packed single-walled carbon nanotubes and their application as super-capacitor electrodes. Nature Mater 5: 987-994.

118. Cheung CL, Kurtz A, Park H, Lieber CM (2002) Diameter-controlled synthesis of carbonnanotubes. J PhysChem B 106: 2429-2433.

119. Buch V, Devlin JP (2003) Water in confining geometries. Springer, Berlin, New York.

120. BylO, LiuJC, WangY, YimWL, JohnsonJK, et al. (2006) Unusual hydrogen bonding in water-filled carbon nanotubes. J Ame Chem Soci 128: 12090-12097.

121. Kotsalis EM, Walther JH, Koumoutsakos P (2004) Multiphase water flow inside carbon nanotubes. InterJ Multi Flow 30: 995-1010.

122. Joseph S, Aluru NR (2008) Why are carbon nanotubes fast transporters of water? Nano Letters 8: 452-458.

123. Sokhan VP, Nicholson D, Quirke N (2002) Fluid flow in nanopores: accurate boundary conditions for carbon nanotubes. J Chem Phys 117: 8531-8539.

124. Thomas JA, Mc Gaughey AJH (2008) Reassessing fast water transport through carbon nanotubes. Nano Letters 9: 2788-2793.

125. Thomas JA, Mc Gaughey AJH, Kuter-Arnebeck O (2010) Pressure-driven water flow through carbon nanotubes: Insights from molecular dynamics simulation. Inter J Therm Sci 49: 281-289.

126. Hashemnia K, FaridM, Emdad H (2011) Dynamical analysis of carbon nanotubes conveying water considering carbon–water bond potential energy and nonlocal effects. Comput Mater Sci 50: 828-834.

127. Balcajin O, Noy A, Fornasiero F, Grigoropoulos CP, Holt JK,et al. (2000) Nanofluidic carbon nanotube membranes: Applications for water purification and desalination. Nanotech Appl Clean Water 77-93.

128. Noy A, Park HG, Fornasiero F, Holt JK, Grigoropoulos CP, et al. (2007) Nanofluidics in carbon nanotubes. Nano Today 2: 22-29.

129. Jia YX, Li HL, Wang M, Wu LY, Hu YD (2010) Carbon nanotube: Possible candidate for forward osmosis. Separation Purification Tech 75: 55-60.

130. Thomas JA, McGaughey AJH, Kuter-Arnebeck O (2010) Pressure-driven water flow through carbon nanotubes: Insights from molecular dynamics simulation. Inter J ThermSci 49: 281-289.

131. Khayet M (2011) Membranes and theoretical modeling of membrane distillation: A review. Advances Colloid Interface Sci 164: 56-88.

132. Mostafavi ST, Mehrnia MR, Rashidi AM (2009) Preparation of nanofilter from carbon nanotubes for application in virus removal from water. Desalination 238: 271-280.

133. Ozoner SK, Yalvac M, Erhan E (2010) Flow injection determination of catechol based onpolypyrrole–carbon nanotube–tyrosinasebiocomposite detector. CurrApplPhys 10:323-328.

134. SinghG, RanaD, MatsuuraT, Ramakrishna S, Narbaitz RM, et al. (2010) Removal of disinfection byproducts from water by carbonized electrospunnano fibrous membranes. Separation Purification Tech 74: 202-212.

135. Qu F, Yang M, Jiang J, Shen G, Yu R (2005) Amperometric biosensor for choline based on layerby-layer assembled functionalized carbon nanotube and polyaniline multilayer film. Anal Biochem 344: 108-114.

136. ChoiJH, JegalJG, KimWN (2006) Fabrication and characterization of multi-walled carbon nanotubes/polymer blend membranes. J Membrane Sci 284: 406-415.

137. Peng FB, Pan FS, Sun HL, Lu LY, Jiang ZY (2007) Novel nanocomposite pervaporation membranes composed ofpoly(vinyl alcohol) and chitosan-wrapped carbon nanotube. J Membrane Sci 300: 13-19.

138. Lu LY, Peng FB, Jiang ZY, Wang J (2006) Pervaporation of benzene/cyclohexane mixtures through poly(vinyl alcohol)/chitosan blend membranes. J Appl Polym Sci 101: 167-173.

139. Prehna K, Adelung R, Heinen M, Nunes SP, Schulte K (2008) Catalytically active CNT–polymer-membrane assemblies: From synthesis to application. J Membrane Sci 321: 123-130.

140. Maab H, Shishatskiy S, Nunes SP (2009) Preparation and characterization of bilayer carbon/polymer membranes. J Membrane Sci 326: 27-35.

141. Gethard K, Sae-Khow O, Mitra S (2011) Water desalination using carbon-nanotube-enhanced membrane distillation. ACS Appl Mater Interfaces 3: 110-114.

142. Shawky HA, Chae SR, LinSH, Wiesner MR (2011) Synthesis and characterization of a carbon nanotube/polymer nanocomposite membrane for water treatment. Desalination 272: 46-50.

143. Celik E, Park H, Choi HY, ChoiHC (2011) Carbon nanotube blended polyethersulfone membranesfor fouling control in water treatment. Water Res 45: 274-282.

144. Celik E, LiuL, Choi HC (2011) Protein fouling behavior of carbon nanotube/polyethersulfone composite membranes during water filtration. Water Res 45: 5287-5294.

145. Madaeni SS, Zinadini S, Vatanpour V (2011) Convective flow adsorption of nickel ions in PVDF membrane embedded with multi-walled carbon nanotubes and PAA coating. Separation Purification Tech 80: 155-162.

146. RoyS, Ntim SA, Mitra S, Sirkar KK (2011) Facile fabrication of superior nanofiltration membranes from interfacially polymerized CNT-polymer composites. J Membrane Sci 375: 81-87.